

DISSECTING THE CIRCUMSTELLAR ENVIRONMENT OF γ -RAY BURST PROGENITORS

JASON X. PROCHASKA¹, HSIAO-WEN CHEN², AND JOSHUA S. BLOOM³
Revised Manuscript: April 22, 2006

ABSTRACT

We investigate properties of the interstellar medium (ISM) in galaxies hosting long-duration γ -ray bursts (GRBs) from an analysis of atomic species (Mg^0 , Fe^0) and excited fine-structure levels of ions (e.g. Si^+). Our analysis is guided primarily by echelle observations of GRB 050730 and GRB 051111. These sightlines exhibit fine-structure transitions of O^0 , Si^+ , and Fe^+ gas that have not yet been detected in intervening quasar absorption line systems. Our results indicate that the gas with large Mg I equivalent width (e.g. GRB 051111) must occur at distances $\gtrsim 50$ pc from GRB afterglows to avoid photoionization. We examine the mechanisms for fine-structure excitation and find two processes can contribute: (1) indirect UV pumping by the GRB afterglow provided a far-UV intensity in excess of 10^6 times the Galactic radiation field; and (2) collisional excitation in gas with electron density $n_e > 10^4 \text{ cm}^{-3}$. The observed abundances of excited ions are well explained by UV pumping with the gas at $r \sim$ a few hundred pc from the afterglow for GRB 051111 and $r < 100$ pc for GRB 050730, without invoking extreme gas density and temperature in the ISM. We show that UV pumping alone provides a simple explanation for all reported detections of excited ions in GRB afterglow spectra. The presence of strong fine-structure transitions therefore may offer little constraint for the gas density or temperature. We discuss additional implications of UV pumping including its impact on chemical abundance measurements, new prospects for observing line-strength variability, and future prospects for studying the gas density and temperature. Finally, we list a series of criteria that can distinguish between the mechanisms of UV pumping and collisional excitation.

Subject headings: gamma-ray bursts

1. INTRODUCTION

Optical afterglows of long-duration γ -ray bursts (GRBs) are almost certainly signposts of extreme star-forming regions at high redshift, because these bursts originate in the catastrophic death of massive stars (e.g. Woosley 1993; Paczyński 1998; Bloom *et al.* 2002; Stanek *et al.* 2003). A detailed study of metal absorption features identified in the circumburst environment can, in principle, yield strong constraints on the progenitor (e.g. Perna & Loeb 1998; Ramirez-Ruiz *et al.* 2005; van Marle, Langer & Garcia-Segura 2005) and offer important insights for understanding mass-loss and chemical feedback during the final evolution stages of massive stars (Wijers 2001; Vink 2005). The benefit of GRBs, which presumably are embedded in environments of Wolf-Rayet stars, is that their optical afterglows provide extremely bright lighthouses at moderate to high redshift, allowing redshifted UV lines to be (albeit transiently) observable with high-resolution spectroscopy.

Past studies based on low-resolution afterglow spectra have been limited to a few diagnostic measurements such as the H I column density, the gas metallicity, and the dust-to-gas ratio (e.g. Savaglio, Fall & Fiore 2003; Vreeswijk *et al.* 2004). In contrast, high-resolution spectroscopy of GRB afterglows has uncovered detailed kinematic signatures, population ratios of excited ions, and chemical compositions of the interstellar medium (ISM) and, perhaps, the circumstellar medium (CSM) of the progenitor star of

the GRB (Vreeswijk *et al.* 2004; Chen *et al.* 2005). These quantities, in principle, permit direct comparisons with simulations describing the evolution history of GRB progenitors (e.g. van Marle, Langer & Garcia-Segura 2005).

An emerging feature of GRB progenitor environments is the presence of strong fine-structure transitions from excited states of C^+ , Si^+ , O^0 , and Fe^+ (Chen *et al.* 2005). Together with their resonance transitions, these fine-structure lines can in principle provide robust constraints on the temperature and density of the gas, as well as the ambient radiation field, independent of the ionization fraction, relative abundances, or metallicity of the gas (Bahcall & Wolf 1968). In particular, detections of Fe II fine structure transitions have only been reported in rare places such as broad absorption-line (BAL) quasars (Hall *et al.* 2002), η Carinae (Gull *et al.* 2005; Nielsen, Gull & Vieira Kober 2005) and the circumstellar disk of β Pictoris (Lagrange-Henri, Vidal-Madjar & Ferlet 1988). The presence of strong Fe II fine-structure lines therefore suggests extreme gas density and temperature in the GRB progenitor environment. In the case of circumburst medium, however, the greatly enhanced radiation field due to the GRB afterglow may also contribute significantly to the formation of these excited ions.

In this paper we present a comprehensive study of the physical properties of the ISM in GRB host galaxies, using absorption lines identified in the echelle spectra of two GRB afterglows, GRB 051111 and GRB 050730 as case studies. We first consider the enhanced radiation field in the circumburst environment due to the progenitor star as well as the optical afterglow, and constrain the distance of the observed neutral gas cloud based on the presence/absence of various atomic lines such as Mg I and Fe I. The dominant species of these elements is in the singly ionized state, because their first ionization potential is less

¹UCO/Lick Observatory; University of California, Santa Cruz; Santa Cruz, CA 95064; xavier@ucolick.org

²Department of Astronomy & Astrophysics; University of Chicago; 5640 S. Ellis Ave., Chicago, IL 60637; hchen@oddjob.uchicago.edu

³Department of Astronomy, 601 Campbell Hall, University of California, Berkeley, CA 94720-3411

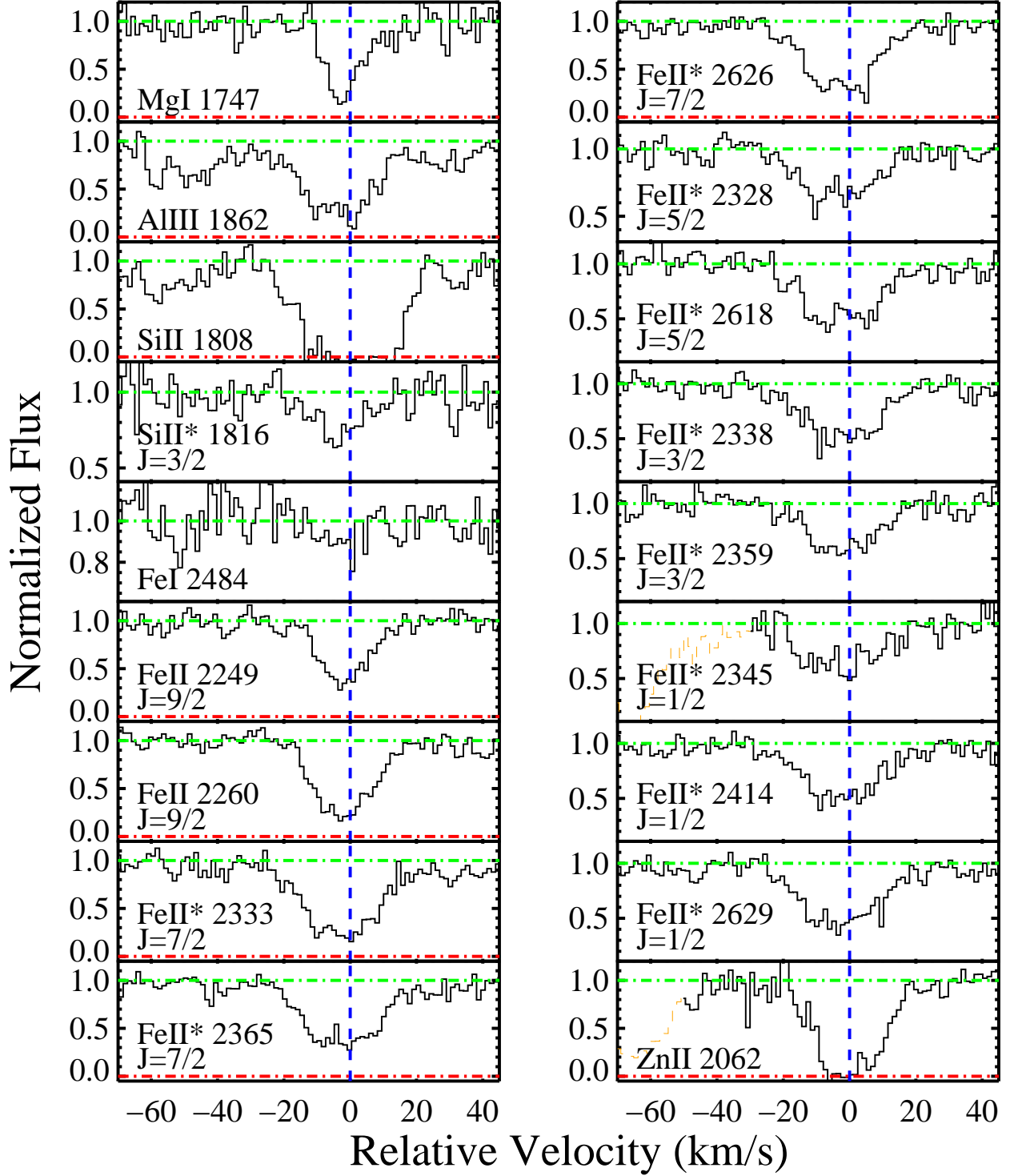


FIG. 1.— Velocity profiles for transitions arising from gas in the host galaxy of GRB 051111. The vertical dashed line at $v = 0$ corresponds to $z = 1.5495$ and the dotted lines indicate blends with coincident transitions.

than 1 Ryd. The presence of strong atomic lines therefore places a lower limit to the distance of the cloud from the afterglow. Next, we investigate the excitation mechanism of the absorbing gas, again taking into account the presence of an intensified radiation field known from afterglow light-curve observations. We compare the predicted population ratios with observations of different ions under photon pumping and collisional excitation scenarios. Although the analysis is based on echelle data obtained for two GRB hosts, we note that the results are applicable to the majority of long-duration GRB's discovered to date. Finally, we discuss additional framework for studying the ISM gas of future events.

The paper is organized as follows. The observations and analysis of echelle spectra for GRB 051111 and GRB 050730 are briefly summarized in § 2. In § 3 we describe the radiation field produced by GRB afterglows. In § 4 we analyze the non-dominant atomic transitions observed in optical afterglow spectra, while § 5 investigates the mechanisms for populating fine-structure states in the dominant ions. In § 6 we consider tests to distinguish between UV pumping and collisional excitation as the principal mechanism for population of fine-structure levels. Finally, § 7 presents a discussion of the results for the specific cases of GRB 051111 and GRB 050730 and, also, generic results for observations of long-duration GRBs. Throughout the paper we assume a cosmology with $\Omega_\Lambda = 0.7$, $\Omega_m = 0.3$ and $H_0 = 70 \text{ km s}^{-1} \text{ Mpc}^{-1}$.

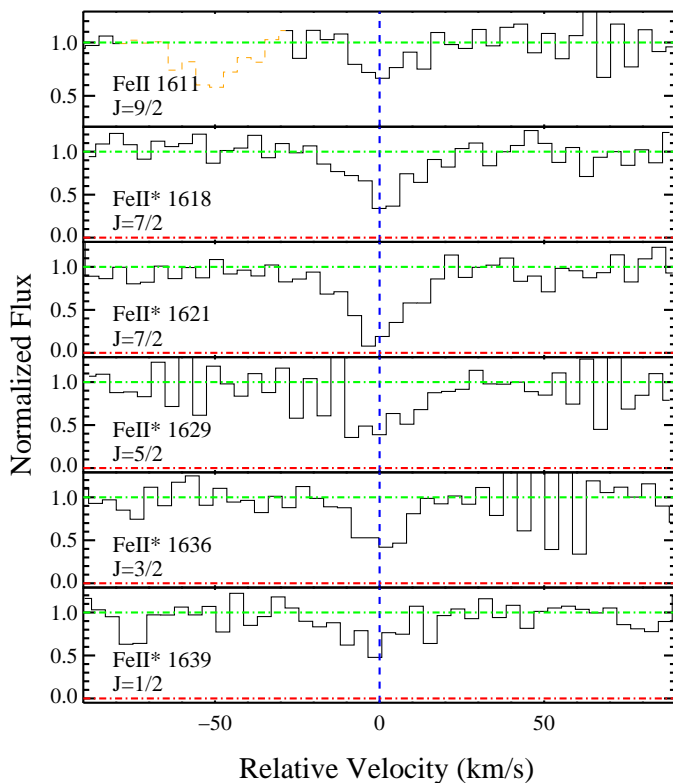


FIG. 2.— Velocity profiles for Fe II transitions arising from gas in the host galaxy of GRB 050730. The vertical dashed line at $v = 0$ corresponds to $z = 3.96855$ and the dotted lines indicate blends with coincident transitions.

2. OBSERVATIONS AND COLUMN DENSITIES

Echelle spectroscopic observations of GRB 051111 were obtained using the High Resolution Echelle Spectrometer (HIRES; Vogt *et al.* 1994) on the Keck I telescope. The observations consisted of three exposures of 1800 s duration each and were initiated by the Keck Observatory staff at UT 07:02:57.92 on 11 November 2005. The spectra⁴ covered a wavelength range from $\lambda = 4165 - 8720 \text{ \AA}$ with a spectral FWHM resolution of $\approx 5 \text{ km s}^{-1}$. A summary of the data reduction is presented in a separate paper (Prochaska *et al.* 2006, in preparation). The final coadded spectrum was normalized to a unit continuum and has $\text{SNR} \approx 15$ per 1.3 km s^{-1} pixel. Figure 1 presents the subset of transitions related to the GRB for the analysis performed in this paper. We (Hill *et al.* 2005) reported the discovery of the redshift $z = 1.549$ for GRB 051111 and preliminary analysis of the results Prochaska (2005). Penprase *et al.* (2005) present an independent analysis of the same data.

Echelle spectroscopic observations of GRB 050730 were obtained using the MIKE echelle spectrograph (Bernstein *et al.* 2003) on the Magellan Clay telescope. The data cover observed wavelengths $\lambda = 3400 - 9000 \text{ \AA}$ at a FWHM $\approx 11 \text{ km s}^{-1}$ dispersion with a typical $\text{SNR} = 12$ per resolution element. A detailed description of the observation and data reduction is presented in Chen *et al.* (2005). In addition to the absorption features presented in Chen *et al.*, here we also present identifications of Fe II transitions from excited fine structure states, $3d^6 4s \text{ } ^6D_{J=5/2,3/2,1/2}$ (Figure 2). Column density measurements of the two GRB sightlines are presented in Tables 1 and 2. The atomic data are taken from Morton (1991); Bergeson & Lawler (1993); Bergeson, Mullan & Lawler (1994, 1996); Tripp, Lu & Savage (1996); Raassen & Uylings (1998); Morton (2003).

Column densities of the unblended transitions were measured using the apparent optical depth method (AODM; Savage & Sembach 1991; Jenkins 1996) over a velocity interval $\pm 40 \text{ km s}^{-1}$ centered at $z = 3.96855$ for GRB 050730 and at $z = 1.54948$ for GRB 051111. In Tables 1 & 2, we list the column densities of individual transitions, the 1σ statistical uncertainty, and the weighted mean. In addition, we report conservative lower limits for saturated transitions and 3σ upper limits for non-detections. No systematic trend between column density and oscillator strength is identified in the measurements, indicating that the absorption lines are well resolved and that the column density measurements are robust. We note, however, that uncertainties in the continuum level are large for features with rest-frame absorption equivalent width $< 10 \text{ m\AA}$. In spite of a formal statistical error < 0.01 dex in several cases, we adopt a minimum 1σ error of 5% in subsequent analyses.

3. RADIATION FIELD PRODUCED BY THE GRB AFTERGLOW

The intimate connection between long-duration GRBs and the end stage of the lifetime of massive stars implies that the gaseous clouds in the vicinity of the progenitor stars have been blasted with intense ultraviolet radiation fields, especially in the early afterglow phase. The radiation field near the GRB, significantly enhanced with re-

⁴The data are publicly available at <http://www.grasp.org>

TABLE 1
IONIC COLUMN DENSITIES FOR GRB051111

Ion	J^a	E_{low} cm ⁻¹	λ (Å)	f	$\log N$	$\log N_{adopt}$
Mg I		0.00	1747.794	0.009080	14.68 ± 0.04	14.68 ± 0.04
		0.00	1827.935	0.023900	> 14.63	
		0.00	2026.477	0.112000	> 14.31	
Al III		0.00	1862.790	0.268000	13.51 ± 0.02	13.51 ± 0.02
Si II	1/2	0.00	1808.013	0.002186	> 16.07	> 16.07
	1/2	0.00	2335.123	0.000004	< 17.27	
	3/2	287.24	1816.928	0.001660	15.00 ± 0.06	15.00 ± 0.06
Fe I		0.00	2484.021	0.557000	< 11.75	< 11.75
Fe II	9/2	0.00	2249.877	0.001821	15.20 ± 0.02	15.24 ± 0.01
	9/2	0.00	2260.780	0.002440	15.28 ± 0.02	
	7/2	384.79	2333.516	0.069170	13.97 ± 0.01	13.98 ± 0.01
	7/2	384.79	2365.552	0.049500	13.99 ± 0.01	
	7/2	384.79	2383.788	0.005175	14.05 ± 0.09	
	7/2	384.79	2389.358	0.082500	14.01 ± 0.02	
	7/2	384.79	2626.451	0.044100	< 14.00	
	5/2	667.68	2328.111	0.035550	13.75 ± 0.02	13.76 ± 0.01
	5/2	667.68	2607.866	0.118000	13.76 ± 0.02	
	5/2	667.68	2618.399	0.050500	13.76 ± 0.02	
	3/2	862.61	2338.725	0.092500	13.54 ± 0.02	13.55 ± 0.01
	3/2	862.61	2359.828	0.057270	13.59 ± 0.02	
	3/2	862.61	2621.191	0.003920	< 13.86	
	1/2	977.05	2345.001	0.157500	13.17 ± 0.03	13.25 ± 0.01
1/2	977.05	2414.045	0.175500	13.25 ± 0.02		
1/2	977.05	2622.452	0.056000	13.28 ± 0.04		
1/2	977.05	2629.078	0.173000	13.28 ± 0.02		
Zn II		0.00	2026.136	0.489000	> 13.60	> 13.71
		0.00	2062.664	0.256000	> 13.71	

^aJ value for ions with excited states. E_{low} is the energy above the ground state.

^bAlthough the statistical uncertainty is as low as 0.01 dex in several cases, we adopt a minimum uncertainty of 5% in the analysis.

spect to the ambient radiation intensity of the host galaxy, modifies the ionization and excitation states of the gas. It is therefore critical to consider first the radiation field produced by the GRB afterglow before then analyzing the absorption-line profiles.

We adopt the afterglow of GRB 051111 as an example. Butler *et al.* (2006) have analyzed the light curve data of this event and characterize the flux of the afterglow at Earth for $t_{obs} > 50$ s as

$$F_{\nu}^{obs} = 1.4 \times 10^{-25} \left(\frac{t_{obs}}{50 \text{ s}} \right)^{-\alpha_t} \left(\frac{\lambda_{obs}}{6588 \text{ Å}} \right)^{-\beta} \text{ erg cm}^{-2} \text{ s}^{-1} \text{ Hz}^{-1} \quad (1)$$

where λ_{obs} and t_{obs} are the observed wavelength and time at Earth. The fading of the afterglow is best-fit with $\alpha_t = 0.87$. The spectral index was estimated to be $\beta = 0.6$ from a fit to the VRIJHK bands, i.e. $h\nu < 6\text{eV}$ at the rest frame of the GRB host. If we assume that this power-law extends to higher energies, then Equation 1 describes the unattenuated flux to energies of several Ryd as a function of time. At some level this radiation field is attenuated by (1) dust and gas in the host galaxy: Lyman limit absorption at $h\nu > 1\text{Ryd}$, (2) dust extinction at all wavelengths, and (3) line opacity by heavy elements and hydrogen Ly-

man series (concentrated at energies $h\nu > 6\text{eV}$). All of these sources of opacity are expected to contribute and we will discuss them when relevant.

We consider three energy intervals important to UV/optical absorption line spectroscopy: (1) a 1Å interval centered at $h\nu = 0.048\text{eV}$ (385cm^{-1}); (2) $8\text{eV} < h\nu < 13.6\text{eV}$; and (3) $1\text{Ryd} < h\nu < 2\text{Ryd}$. The first is set by the energy necessary to populate the first excited state $J = 7/2$ of Fe^+ from its ground state $J = 9/2$ via a magnetic dipole transition. The 1Å interval is chosen to roughly coincide with the width of the line-profile which is set by the gas kinematics along the GRB sightline. The second interval is a measure of the far-UV radiation field. To provide comparison with the Milky Way, we adopt Habing's constant $G_0 = 1.6 \times 10^{-3} \text{ erg cm}^{-2} \text{ s}^{-1}$, which roughly corresponds to the Galactic far-UV intensity (Habing 1968). More recent estimates place the Galactic radiation field at $\approx 1.7G_0$ (Gondhalekar, Phillips & Wilson 1980). The third energy interval characterizes the radiation field responsible for ionizing hydrogen atoms.

In Figure 3 we plot the number of photons per cm^2 emitted by the afterglow of GRB 051111 from $t = t_{obs}/(1+z) = 19\text{s}$ to 1506s versus the radial distance r from the GRB in

TABLE 2
IONIC COLUMN DENSITIES FOR GRB 050730

Ion	J ^a	E_{low} cm ⁻¹	λ (Å)	f	log N	log N_{adopt}
C I	1/2	0.00	1277.245	0.096650	< 13.37	< 13.37
	1/2	0.00	1656.928	0.140500	< 13.47	
O I	1/2	0.00	1302.168	0.048870	> 15.27	> 15.27
	1/2	0.00	1355.598	0.000001	< 18.09	
	2/2	158.26	1304.858	0.048770	> 14.94	> 14.94
	4/2	226.98	1306.029	0.048730	> 14.61	> 14.61
Si II	1/2	0.00	1260.422	1.007000	> 14.08	> 14.69
	1/2	0.00	1304.370	0.094000	> 14.69	
	1/2	0.00	1526.707	0.127000	> 14.55	
	1/2	0.00	1808.013	0.002186	< 15.59	
	3/2	287.24	1264.738	0.903400	> 14.03	< 16.03
	3/2	287.24	1265.002	0.100400	> 14.56	
	3/2	287.24	1309.276	0.146800	> 14.28	
	3/2	287.24	1817.451	0.000129	< 16.03	
Fe II	9/2	0.00	1608.451	0.058000	> 14.72	14.98 ± 0.12
	9/2	0.00	1611.200	0.001360	14.98 ± 0.12	
	7/2	384.79	1618.468	0.021400	14.26 ± 0.06	14.29 ± 0.04
	7/2	384.79	1621.686	0.038100	14.34 ± 0.07	
	5/2	667.68	1629.160	0.036700	14.12 ± 0.07	14.12 ± 0.07
	3/2	862.61	1634.350	0.020500	13.95 ± 0.11	13.92 ± 0.06
	3/2	862.61	1636.331	0.040500	13.91 ± 0.07	
	1/2	977.05	1639.401	0.057900	13.65 ± 0.07	13.65 ± 0.07

^aJ value for ions with excited states. E_{low} is the energy above the ground state.

^bAlthough the statistical uncertainty is as low as 0.01 dex in several cases, we adopt a minimum uncertainty of 5% in the analysis.

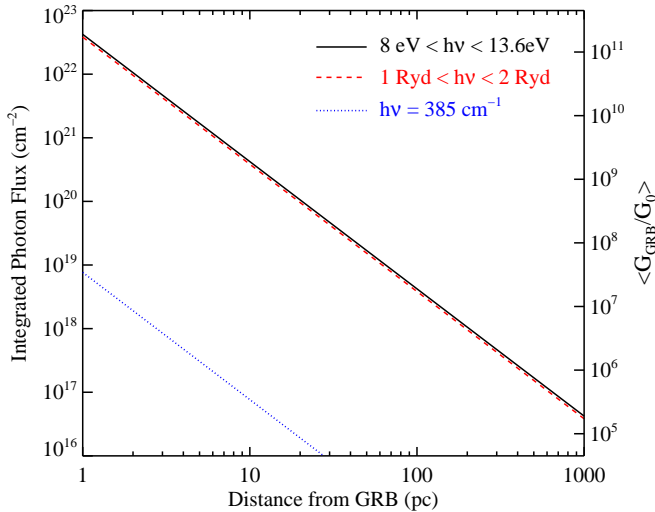


FIG. 3.— Integrated, unattenuated flux of photons emitted by the afterglow of GRB 051111 from $t = 19.6$ to 1506 s with energies in three intervals: (1) Hydrogen ionizing radiation ($1\text{Ryd} < h\nu < 2\text{Ryd}$; red curve); (2) far-UV radiation ($8\text{eV} < h\nu < 13.6\text{eV}$; black curve); (3) photons which would excite Fe^+ from the $J = 9/2$ to $J = 7/2$ level (a 1\AA interval centered at $h\nu = 0.048\text{eV}$; blue curve). The radial dependence is simple r^2 dimming. The right axis presents the time-averaged intensity of the far-UV radiation field G_{GRB} relative to Habing's constant G_0 .

the rest-frame of the GRB host. For the $E = 385\text{ cm}^{-1}$ photons, we assume a 1\AA interval. Similar to previous work (e.g. Perna & Loeb 1998; Draine & Hao 2002), we find that in the absence of intervening gas and dust the GRB afterglow would initiate a burning front that would ionize an H I column of several 10^{22} cm^{-2} atoms at $r = 1\text{ pc}$. As impressive, one notes that the far-UV intensity is over 10^5 times larger than the ambient Milky Way field even at $r = 1\text{ kpc}$. Despite its transient nature, the afterglow emits more UV photons in a few minutes than the entire galaxy in one year (assuming a star formation rate $\text{SFR} = 20\text{ M}_\odot\text{ yr}^{-1} = 1.6 \times 10^{28}\text{ erg s}^{-1}\text{ Hz}^{-1}$; e.g. Kennicutt 1998).

The estimated strength of the radiation field due to this afterglow has three important implications, which are applicable to many other GRBs. First, if neutral gas were present at $r < 1\text{ pc}$ of the progenitor prior to the burst (which is unlikely assuming significant UV luminosity from the GRB progenitor), the implied mean hydrogen density $\langle n_H \rangle$ would have to exceed 10^4 cm^{-3} for any neutral gas to survive the burst. At $r > 10\text{ pc}$, however, significant absorption is still expected from neutral gas if $\langle n_H \rangle$ is greater than 10 cm^{-3} . Second, neutral atoms with ionization potential less than 1 Ryd (present within the spectrum of GRB 051111) are very unlikely to survive the first few hundred seconds (§ 4). Third, the intensity of the radiation field at even 1 kpc is large enough that photon pumping of fine-structure states cannot be ignored. In the following sections, we will consider photon pumping and

discuss constraints on the distance to the progenitor stars, the gas density and temperature of the observed gas.

4. GASEOUS PROPERTIES AS CONSTRAINED BY ATOMIC SPECIES

By definition, neutral hydrogen gas clouds are opaque to radiation with $h\nu > 1\text{Ryd}$ and transparent to lower energy photons (aside from opacity by the Lyman series). Because the first ionization potential of most elements is less than 1 Ryd, the dominant species of these elements is singly ionized gas, e.g. Fe^+ , Si^+ , and Mg^+ . However, the atomic phase is detected in trace quantities in various gaseous phases of the ISM of nearby galaxies (e.g. Frisch *et al.* 1990; Welty, Hobbs & Morton 2003). One of the most common examples is Mg^0 . Surveys of Mg I lines in the Milky Way have revealed this atom in both cold and warm phases of the neutral ISM (e.g. Frisch, York & Fowler 1987; Frisch *et al.* 1990). In addition, atomic Mg is also often detected in quasar absorption line systems exhibiting strong Mg II absorption (e.g. Steidel & Sargent 1992; Churchill *et al.* 2000). This includes damped Ly α systems at all redshifts (Rao & Turnshek 2000; Prochaska & Wolfe 2002). The frequent presence of Mg^0 is driven by a relatively low photoionization cross-section and modest recombination coefficients. At low temperature radiative recombination dominates while at $T \gtrsim 5000\text{K}$ dielectronic recombination becomes significant, allowing Mg I absorption to be observed from even partially ionized regions (York & Kinahan 1979).

In this section, we examine the presence/absence of Mg^0 (IP=7.64eV) and Fe^0 (IP=7.90eV) along the GRB 051111 sightline. Although the results are directed to the gas in this GRB host galaxy, neutral species have been reported in other GRB afterglow spectra (e.g. Barth *et al.* 2003; Foley *et al.* 2005) and our conclusions are qualitatively applicable to those cases. One can also generalize the results to additional atomic species, e.g., Si^0 and C^0 .

Column density measurements for the atomic species shown in Figure 1 are presented in Table 1. We detect several transitions of Mg I but no Fe I transition. The Mg^0 column density for the host galaxy of GRB 051111 may be the largest ever recorded outside the Milky Way. Based on the kinematics of the Mg I profile and its large column density, we argue that this atomic gas is co-spatial with the majority of low-ion absorption observed along the sightline. As such, we will treat the Mg^0 , Mg^+ , Fe^0 , and Fe^+ gas to arise from a single cloud within the ISM of the galaxy. While Mg^0 atoms are also likely to reside in the halos of galaxies (e.g. Charlton & Churchill 1998), the expected column density is small and should show significantly different kinematics.

4.1. Distance of Neutral Gas to the GRB

Even if physical conditions in the ISM of the GRB host galaxy support a significant Mg^0 column density, the enhanced far-UV radiation from the GRB afterglow can burn away the gas even at large distance from the burst. Observations of Mg^0 , therefore, can place a lower limit to the distance of the neutral gas to the burst.

As an estimate to this lower limit, we calculate the distance r_{min} at which 99.99% of the Mg^0 atoms would be ionized by the GRB afterglow. At this level of photoionization, one would not expect to detect even the strong

Mg I 2852 transition. For an optically thin slab, r_{min} corresponds to the distance at which the gas experiences an integrated photon surface density $N_\gamma = \ln(10^4)/\sigma_{ph}$. For a total number of ionizing photons ϕ , the distance is

$$r_{min} = 100 \times \left[\frac{\phi \sigma_{ph}}{1.1 \times 10^{43}} \right]^{\frac{1}{2}} \text{ pc} \quad . \quad (2)$$

We adopt the functional form given by Verner *et al.* (1996) for the photoionization cross-section of Mg^0 , $\sigma_{ph}^{\text{Mg}^0}(E)$. This function peaks at the ionization potential $\sigma_{ph}^{\text{Mg}^0}(E = 7.64\text{eV}) = 1.7 \times 10^{-18} \text{ cm}^2$ and declines sharply with increasing energy. We assume a value $\sigma_{ph}^{\text{Mg}^0} = 10^{-18} \text{ cm}^2$ (corresponding to $E \approx 8.5\text{eV}$) as a conservative estimate of the cross-section. For GRB 051111, we calculate a time-averaged luminosity density at $h\nu = 8.5\text{eV}$, $\langle L_\nu \rangle_t = 6.4 \times 10^{31} \text{ erg s}^{-1} \text{ cm}^{-2} \text{ Hz}^{-1}$ over $t = 20 - 1000\text{s}$, leading to a mean total photon number $\phi = 2 \times 10^{60}$ at 8.5 eV. Substituting $\sigma_{ph}^{\text{Mg}^0}$ for σ_{ph} in Equation (2) yields $r_{min} = 46 \text{ pc}$ for the neutral gas observed in the GRB 051111⁵. The presence of strong Mg I absorption transitions at $t = 1500\text{s}$ after the burst therefore suggests that the neutral gas is located *at least* 50 pc away from the afterglow.

TABLE 3

CONSTRAINTS ON CIRCUMBURST DISTANCES OF OBSERVED NEUTRAL GAS

GRB	z	α	β	Ref	$\log L_\nu^a$ (cgs)	r_{MgI}^b (pc)	r_{excite}^c (pc)
010222	1.477	0.80	0.89	1	31.39	40	190
020813	1.254	0.85	0.92	2	31.09	30	140
021004	2.328	1.05	1.05	3	32.21	140	620
030323	3.372	1.56	0.89	4	32.85	540	2330
030329	0.169	1.10	1.00	5	31.38	60	250
050408	1.236	0.79	1.30	6	29.93	10	40
050730	3.969	0.30	1.80	7	32.16	70	340
050820	2.615	0.95	1.00	8	31.97	100	430
051111	1.549	0.87	0.60	9	31.32	40	180
060206	4.048	1.01	0.51	10	32.41	170	730

^aSpecific luminosity of the GRB afterglow at $t = 1000\text{s}$ for $\nu = 8\text{eV}/h$.

^bRadius from the GRB afterglow where 99.99% of Mg^0 atoms would be ionized.

^cApproximate radius where a column of 10^{14} cm^{-2} Si^+ ions would experience one excitation per minute per ion.

Note. — We caution that the values listed in this Table should be considered rough estimates of the light curves. The flux of the GRB observed at Earth is given by $F_\nu = (L_\nu/4\pi d_L^2/[1+z])(t/1000)^\alpha (\nu/1.7 \times 10^{15} \text{ Hz})^\beta$. We have not corrected for the fluxes for dust extinction in the host galaxy.

References. — 1: Mirabal *et al.* (2002); 2: Barth *et al.* (2003); 3: Mirabal *et al.* (2003); 4: Vreeswijk *et al.* (2004); 5: Lipkin *et al.* (2004); 6: Foley *et al.* (2005); 7: Chen *et al.* (2005); 8: Cenko & Fox (2005); 9: Butler *et al.* (2006); 10: Perley *et al.* (2006)

A stronger constraint can be placed on the minimum distance from the GRB by evaluating time variations in the

⁵Note that one can ignore recombination provided that the density is not extraordinary, i.e. $n_e < 10^9 \text{ cm}^{-3}$.

Mg⁰ column density (Mirabal *et al.* 2002). In this case, the result is independent of the total Mg⁰ column density prior to the GRB. For GRB 051111, we set an upper limit to the decline in $N(\text{Mg}^0)$ over the central 40km s⁻¹ interval to be less than 25% during a $\Delta t_{\text{obs}} = 1800$ s exposure. The number of photons emitted over the time interval $t_{\text{obs}} = (3840 + 900)$ s to $t_{\text{obs}} = (3840 + 2700)$ s is $\phi = 2.3 \times 10^{57}$. Therefore, we find a lower limit to the separation based on the absence of line-strength variability to be

$$r_{\text{min}}^v = \left[\frac{\phi \sigma_{ph}^{\text{Mg}^0}}{4\pi \ln(N_i/N_f)} \right]^{\frac{1}{2}} > 80 \text{ pc} \quad (3)$$

for $N_f > 0.75N_i$. This is in good agreement with our estimate for r_{min} from above. Note that if we were able to place an upper limit to the variability of 5% then r_{min}^v would double.

We present estimates of r_{min} for several other GRB assuming Equation 2, together with the estimated parameterization of the light curves shown in Table 3. The results for GRB 020813 and GRB 050408 are notable because those sightlines also exhibit significant Mg⁰ gas. Our analysis demonstrates that the conditions for GRB 051111 are not atypical. A generic result of our analysis is that Mg⁰ absorption identified in GRB spectra must correspond to gas at distances $\gtrsim 100$ pc from the afterglow.

4.2. Electron Density

In the previous section, we have argued that the very presence of Mg⁰ gas or lack of time variability in its column density indicate the gas is located at large distance from the GRB afterglow. In this case, one can examine the gas under the assumptions of steady-state balance and photoionization equilibrium. Considering together the presence (or absence) of atomic species like Mg⁰ and Fe⁰ in a neutral hydrogen gas leads to constraints on the ratio of the electron density to the intensity of ambient far-UV radiation. For the ionization balance of Mg⁰ and Mg⁺, we express photoionization equilibrium in terms of the column density ratios (Appendix A),

$$n_e = \frac{N(\text{Mg}^0) \Gamma(\text{Mg}^0)}{N(\text{Mg}^+) \alpha^{\text{Mg}^+}(T)}, \quad (4)$$

where $\Gamma(\text{Mg}^0) = \text{Const.} \times \sigma_{ph}(\text{Mg}^0) \times G/G_0$ represents the photoionization rate of Mg⁰ and $\alpha^{\text{Mg}^+}(T)$ is the total recombination coefficient dependent upon the gas temperature T . Equation (4) demonstrates that observations of the relative ionization fraction for a single heavy element constrain $n_e \times (G/G_0)^{-1}$ at a given temperature.

For GRB 051111, the Mg II doublet is highly saturated in the echelle data and only a lower limit can be placed. We can estimate, however, a conservative upper limit to $N(\text{Mg}^+)$ from the observed column density of Zn⁺. First, we assume relative solar abundances for Zn and Mg. Next, we increment the observed $\log N(\text{Zn}^+)$ by 1 dex to account for both line-saturation and a nucleosynthetic enhancement relative to solar. This treatment presumes the Mg⁰ gas is co-spatial with the Mg⁺ ions inferred from Zn⁺, which is supported by the kinematic characteristics of the various line profiles (Figure 1). Finally, we derive a conservative lower limit to the ratio $N(\text{Mg}^0)/N(\text{Mg}^+) > 10^{-2.8}$.

The corresponding lower limit of $n_e \times (G/G_0)^{-1}$ as a function of T is shown in the solid, blue curve in Figure 4.

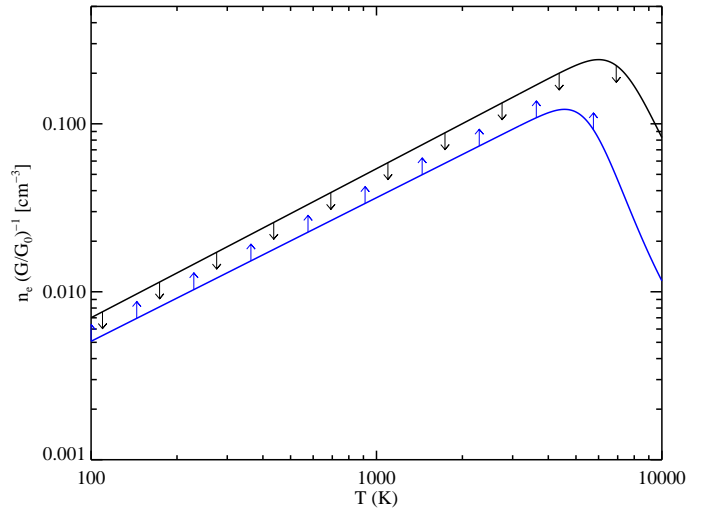


FIG. 4.— Constraints on the ratio of electron density n_e to the ambient far-UV intensity $(G/G_0)^{-1}$ as a function of the gas temperature. The black curve set an upper limit based on the non-detection of atomic Fe. The blue curve set a lower limit based on the detection of atomic Mg and a conservative upper limit to the column density of Mg⁺.

We repeat this analysis for the observed ratio Fe⁰/Fe⁺. At $T < 8000$ K, radiative recombination dominates and we have

$$n_e = \frac{N(\text{Fe}^0) \Gamma(\text{Fe}^0)}{N(\text{Fe}^+) \alpha_r^{\text{Fe}^+}(T)}. \quad (5)$$

The absence of Fe⁰ places an upper limit on the column density ratio $N(\text{Fe}^0)/N(\text{Fe}^+) < 10^{-3}$, which in turn leads to an upper limit of $n_e \times (G/G_0)^{-1}$ as shown in the solid, black curve in Figure 4.

Figure 4 allows us to roughly estimate the electron density of the gas for a known ambient radiation field G . If the GRB progenitor was located within a star forming region, then the ambient far-UV radiation field could be large. Observations of known GRB host galaxies at $z > 1$ show a mean star formation rate integrated throughout the host ISM of $\text{SFR} \sim 10 M_\odot \text{yr}^{-1}$ (Christensen, Hjorth & Gorosabel 2004; Le Floc'h *et al.* 2006). Even if all the star formation were concentrated in a single cloud, the mean intensity at 1 kpc is $G/G_0 \approx 100$. At $T < 10000$ K, we therefore estimate $n_e = 1 - 10 \text{ cm}^{-3}$. Assuming an ionization fraction of $x \equiv n_{\text{H}^+}/n_{\text{H}} = 10^{-2}$, we estimate the hydrogen volume density $n_{\text{H}} = 100 - 1000 \text{ cm}^{-3}$; this value is comparable to what is observed in the Galactic H II regions or giant molecular clouds. To estimate the size of the neutral gaseous cloud, we adopt the observed $\log N(\text{Zn}^+) > 13.7$ and assume a solar metallicity to infer $\log N_{\text{HI}} > 21$. We derive a cloud size of $l \equiv N_{\text{HI}}/n_{\text{H}} > 3$ pc. Lower metallicity would imply a higher N_{HI} and a larger size for the cloud.

5. IMPLICATIONS FROM OBSERVATIONS OF FINE-STRUCTURE TRANSITIONS

Additional constraints on the gas density, UV radiation intensity, and the spectral shape of the afterglow emission

can be learned from comparing the line strengths of different fine structure lines (e.g. Bahcall & Wolf 1968). Although Fe II and Si II fine-structure transitions have yet to be observed in intervening quasar absorption line systems (e.g. Howk, Wolfe & Prochaska 2005), they appear to be a generic feature in the GRB host environment. Their presence indicates unique physical conditions in the ISM hosting the GRBs.

The excited states can be produced through either photon pumping or collisional excitations. In this section, we will investigate these various excitation mechanisms. Specifically, we will consider for photon pumping (1) direct excitation by IR radiation from sources local to the gas⁶ and (2) fluorescence following excitations by ultraviolet photons. For collisional excitations, we will discuss (3) collisions with charged particles, primarily electrons, and (4) collisions with neutral hydrogen. Although the photon pumping processes are generally weak in typical astrophysical environments, the radiation field of the GRB afterglow is extreme (Figure 3) and can dominate the excitation processes.

To estimate the strength of the afterglow UV radiation field at the location of the absorbing gas in GRB 051111, for example, we adopt the minimum distance from § 4.1 and Equation 3, $r_{\min} = 80$ pc. We conclude that the majority of Fe⁺ resides at a distance of 80 pc or greater from the afterglow. At $r = 80$ pc, the FUV radiation field is still $> 10^7 G/G_0$ (Figure 3), stronger than that observed for intense star-forming regions.

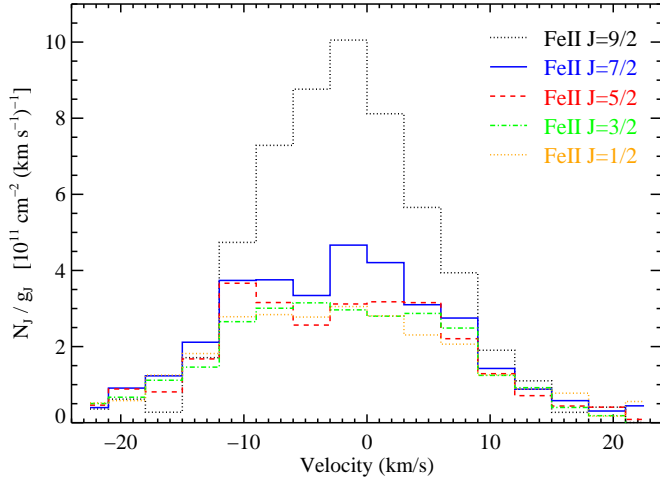


FIG. 5.— Average apparent optical depth profiles normalized by the degeneracy ($g_J \equiv 2J + 1$) of the five $6D_{9/2}$ levels of Fe⁺ for GRB 051111. One notes that the excited states track one another closely but that the ground state exhibits greater optical depth at $v > 0$ km s⁻¹ relative to the excited states. Also note that the g_J -normalized column densities of the $J = 9/2$ ground-state level are scaled down by a factor of 20 to enable comparison with the excited states.

Figure 5 shows the apparent optical depth profiles of the five a^6D levels of Fe⁺ from GRB 051111 normalized by their degeneracy $g_J \equiv 2J + 1$. We emphasize three

⁶Note that the CMB temperature and photon density at $z = 1.54948$ cannot account for significant external IR pumping.

observations from the Figure. First, the velocity profiles of the excited states (color histograms) track each other very closely. Second, the g_J normalized profiles of the excited states have roughly the same value. Indeed, the total column densities of the $J = 7/2$ to $J = 1/2$ states are roughly proportional to the degeneracy $N_J \propto g_J$ with a modest but statistically significant decrease with increasing J . To populate the excited levels according to their degeneracy implies a saturated excitation process, i.e., an excitation rate that is much faster than the spontaneous decay rate. Therefore, it is unlikely the physical conditions vary considerably with velocity and we can integrate the profiles for the excited states over the entire velocity range to consider the total column densities. Lastly, the ground state ($J = 9/2$) exhibits a discrepant g_J normalized profile from the excited states, containing $\approx 20\times$ higher column density than the value expected from the population of the excited levels. The ground level is clearly not populated according to its degeneracy relative to the excited states.

Because no viable excitation mechanism will populate only the excited states according to g_J , we conclude that the sightline has intersected at least two phases of gas: one with minimal excitation which contains roughly 95% of the ground-state gas and one where all of the a^6D levels are roughly populated according to g_J . These two phases could be embedded within one another (e.g. a dense core within a less dense cloud) or even represent separate layers of the same clump. Figure 5 offers additional kinematic evidence for two distinct phases; one observes that the ground-state profile is more sharply peaked at $v = 0$ km s⁻¹ than the excited states. For these reasons, in the following discussion we will not include observational constraints drawn from the ground states of Si⁺, Fe⁺, or O⁰. While Figure 5 presents only the results for GRB 051111, we note that the data from GRB 050730 is qualitatively similar; the excited states are populated according to g_J and the ground state shows a significant overabundance (Table 2).

5.1. Direct IR Pumping

We first examine the population ratios of the excited states under the scenario of excitation by IR photons. Direct IR pumping can populate the excited states of Si⁺, Fe⁺, and O⁰ through forbidden magnetic dipole transitions. Because these transitions have selection rules $\Delta J = 0, \pm 1$, excited states beyond the first level must be populated by an upward cascade of transitions. If IR pumping dominates, then the excitation of level j relative to the ground-state i is given by

$$\frac{N_j}{N_i} = \frac{g_j}{g_i} \frac{N_\nu^\gamma}{1 + N_\nu^\gamma} \quad (6)$$

where N_ν^γ is the number of photons at the appropriate frequency ν

$$N_\nu^\gamma = \frac{I_\nu \lambda^3}{8\pi h c} \quad (7)$$

To explore the process of IR pumping, we consider the spectrum of the radiation field required to reproduce the observed column density ratios between the excited states of Fe⁺ for GRB 051111. We ignore the $J = 9/2$ state because $\approx 95\%$ of the ground-state ions must arise in a distinct region from the excited Fe⁺ gas. Figure 6 presents

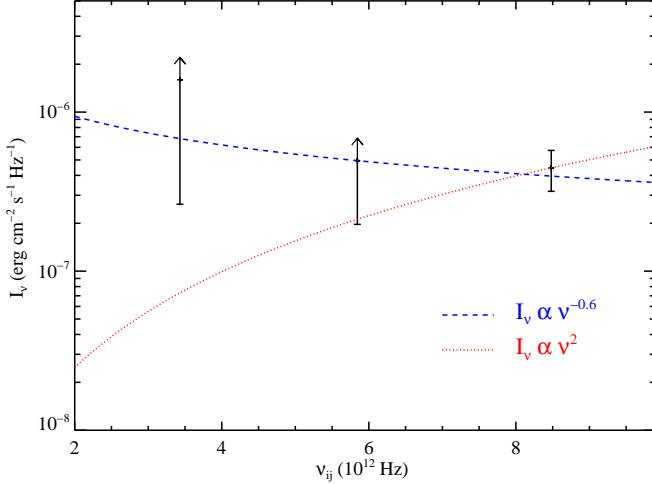


FIG. 6.— Calculated intensity of the radiation field required to reproduce the relative populations of the $J = 7/2, 5/2, 3/2$ and $J = 1/2$ levels of Fe^+ for GRB 051111 via direct IR pumping (magnetic dipole transitions). The error bars reflect $1\text{-}\sigma$ uncertainties in the ratios. For the upper two transitions (lower frequency), the observed ratios are within 1σ of satisfying $n_i g_j = n_j g_i$. Therefore, there is no formal upper bound to I_ν and we show the central value but also express the result as a lower limit. The blue dashed curve qualitatively represents the flux from the GRB afterglow, i.e. a radiation field with $I_\nu \propto \nu^{-0.6}$. The red dotted curve shows the radiation field of a thermal source with $I_\nu \propto \nu^3$. The latter radiation field is ruled out by the observations.

the intensities inferred from the observed population ratios of two adjacent levels ($J = 7/2 \rightarrow 5/2$, $J = 5/2 \rightarrow 3/2$, and $J = 3/2 \rightarrow 1/2$) versus the corresponding excitation frequency. The error bars reflect $1\text{-}\sigma$ uncertainties in the ratios. For the upper two transitions, the observed ratios are within 1σ of satisfying $n_i g_j = n_j g_i$. Therefore, there is no formal upper bound to I_ν and we show the central value but also express the result as a lower limit.

Superimposed on the plot are the predictions for two radiation fields with $I_\nu \propto \nu^2$ (e.g. a thermal spectrum with $T > 200\text{K}$) and $I_\nu \propto \nu^{-0.6}$ (the optical afterglow spectrum; Butler et al. 2006). The thermal radiation field is ruled out at high confidence, whereas the GRB spectrum (or a slightly steeper spectrum, $\beta \approx 0$, which might be appropriate for these low frequencies) is acceptable. For GRB 050730, where the population of the excited levels are all consistent with g_J due to large measurement uncertainties, the data are consistent with a constant $I_\nu > 10^{-6} \text{ erg s}^{-1} \text{ cm}^{-2} \text{ Hz}^{-1}$ over $\nu = 2 - 9 \times 10^{12} \text{ Hz}$. This is higher than any reasonable IR source (i.e. dust) in even the most intense star-forming regions, and could only be produced by the GRB afterglow.

Next, we estimate the number of Fe^+ ions that were excited by IR photons from the afterglow prior to the start of the echelle observations. We calculate the excitation rate as a function of distance from the afterglow, taking into account the spontaneous decay rate of the excited levels. The spontaneous decay coefficient of the first excited level is $A_{7/2,9/2} = 2.12 \times 10^{-3} \text{ s}^{-1}$ giving a decay time of 8 minutes and an oscillator strength of

$$f_{ji} = \frac{A_{ji} t_0}{\frac{1}{2} \alpha^3 \frac{g_i}{g_j} E_{ji}^2} = 2.16 \times 10^{-8} \quad (8)$$

where $t_0 = 2.419 \times 10^{-17} \text{ s}$, α is the fine-structure constant, and E_{ji} is the transition energy (Ryd). For a gas ‘cloud’ with column density $N(\text{Fe}^+) = 10^{15} \text{ cm}^{-2}$ and Doppler parameter $b = 15 \text{ km s}^{-1}$, the optical depth at line center is

$$\tau_0 = \frac{1.5 \times 10^{-2} N \lambda f_{ji}}{b} = 5.6 \times 10^{-4} \quad (9)$$

with all quantities expressed in cgs units. The estimated optical depth indicates that the gas is optically thin to the IR photons. To estimate the number of photons absorbed by the cloud per decay time, we calculate the equivalent width in the optically thin limit

$$W_\lambda = 8.85 \left(\frac{N}{10^{15} \text{ cm}^{-2}} \right) \left(\frac{\lambda}{1000 \text{ \AA}} \right)^2 f_{ji} = 13 \text{ m\AA} \quad (10)$$

Figure 3 shows the number of IR photons emitted from $t_{\text{obs}} = 50 \text{ s}$ to 3840 s with energy $E_{9/2,7/2} = 385 \text{ cm}^{-1}$ in a 1\AA window. The number of excitations per ion⁷ per decay time is

$$n_{\text{excite}}^{\text{IR}} = \left(\frac{W_\lambda}{1 \text{ \AA}} \right) \left(\frac{N_\nu^\gamma}{N_{\text{ion}}} \right) \left(\frac{\Delta t_{\text{decay}}}{\Delta t} \right) \left(\frac{r}{1 \text{ pc}} \right)^{-2} = 26 \left(\frac{r}{\text{pc}} \right)^{-2}, \quad (11)$$

where $N_\nu^\gamma = 10^{18.8}$ photons per cm^{-2} , $n_{\text{ion}} = 10^{15}$ ions per cm^{-2} , $\Delta t_{\text{decay}} = 480 \text{ s}$, $\Delta t = \Delta t_{\text{obs}} / (1+z) = 1487 \text{ s}$.

According to Equation 11, there is a sufficient photon flux at $r = 1 \text{ pc}$ from GRB 051111 to excite the $\text{Fe II } J = 7/2$ level prior to the onset of the echelle observations but the photon flux is too low at $r = 80 \text{ pc}$. Our analysis therefore indicates that IR pumping is unlikely the primary mechanism for producing the excited ions found in GRB 051111. Furthermore, in the next sub-section we will show that the excitation rate by UV pumping is orders of magnitude higher than IR pumping. Therefore, we conclude that *IR pumping is an unimportant excitation mechanism for gas observed in GRB afterglow spectra.*

5.2. Indirect UV Pumping

The fine-structure states of Fe^+ , Si^+ , and O^0 ions can also be populated by the absorption of a UV photon to an upper level, followed by spontaneous radiative decay to an excited level of the ground term. Requiring electric dipole transitions, the maximum angular momentum change is $|\Delta J_{\text{max}}| = 2$. Therefore, one requires a series of excitations to populate the $J = 3/2, 1/2$ levels of Fe^+ , and only a single absorption for the Si^+ ion and O^0 atom. The analysis of UV pumping is similar to IR pumping, although it requires a careful consideration of all the upper levels. To perform the calculation, we adopt the software packaged Popratio developed by Silva & Viegas (2001, 2002) which incorporates modern atomic data for these various ions.

Similar to the treatment of IR pumping, we investigate (1) whether the observations describe a physically sensible radiation field; and (2) whether the pumping rate is sufficient to excite a significant column of gas prior to the start of spectroscopic observations assuming the GRB afterglow is the radiation source. We first examine the radiation field required to explain the observed population ratio of different excited states.

⁷Note that the rate is independent of the number of ions assumed here provided the optical depth remains small.

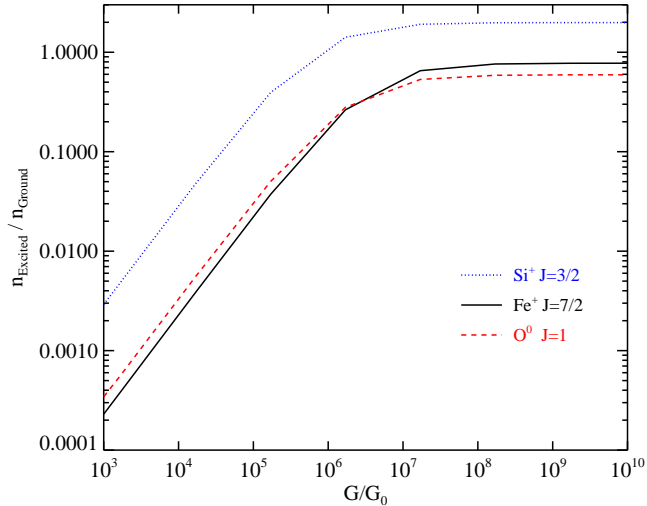


FIG. 7.— Indirect UV pumping of the first excited state relative to the ground state for Si^+ , Fe^+ , and O^0 versus the far-UV intensity (normalized to Habing’s constant, G_0). At large intensity, the levels saturate to ratios according to their relative degeneracies g_J . Note that Si^+ exhibits a much higher excitation ratio than the other gas.

Figure 7 shows the excitation of the first excited states of Fe^+ , Si^+ , and O^0 relative to the ground state as a function of the far-UV intensity in terms of Habing’s constant $G_0 = 1.6 \times 10^{-3} \text{ erg cm}^{-2} \text{ s}^{-1}$. The results are drawn from Popratio calculations assuming physical characteristics for the gas such that UV pumping dominates (i.e. $n_e = 1 \text{ cm}^{-3}$). We emphasize three points from the figure. First, all of the excited states saturate at $G/G_0 > 10^7$. At these intensities, the levels are populated only according to the degeneracy of the excited state relative to the ground state and the differences between ions reflect the various J values. Second, the excitation fraction is negligible and is nearly proportional to G for $G/G_0 < 10^5$, beyond which pumping induced excited ions become dominant. Finally, Si^+ exhibits ≈ 10 times higher excitation fraction than Fe^+ and O^0 for the same G/G_0 values. This is partly due to the fact that the Si II levels are inverted (g_J for the excited state is twice that of the ground state), but also arises from the detailed atomic physics of the upper levels⁸.

If we adopt a minimal excitation for Fe^+ , then for GRB 051111 only roughly 7% of the observed $N_{J=9/2}(\text{Fe}^+)$ originates in the excited phase, then our observations imply a UV radiation field of $G/G_0 > 10^7$ under a steady-state assumption (Figure 7). At this radiation intensity, we also infer a population ratio for Si^+ , $n_{J=3/2}/n_{J=1/2} \sim 2$, indicating that roughly 5% of the observed ground-state Si^+ originates in the excited phase. This exercise shows that roughly the same fraction of the observed Fe^+ and Si^+ ions have been excited toward GRB 051111 under the indirect UV pumping mechanism.

Examining the far-UV radiation field of a GRB afterglow (Figure 3), we note that the unattenuated intensity is sufficient in steady-state conditions to excite all of the ions out at even several hundred parsecs where $G/G_0 > 10^6$.

⁸It is not an effect of UV absorption strengths; all of the ions exhibit a significant number of resonance transitions in the far-UV.

In particular, the luminosity of the GRB exceeds that for star-forming regions with $\text{SFR} = 100 M_\odot \text{ yr}^{-1}$ by a factor of 1000. Therefore, if the excitation rate of the ions is large on the time-scale of the afterglow observations (e.g. minutes to hours), then the burst should excite Fe^+ , Si^+ , and O^0 via indirect UV pumping.

The excitation rate due to fluorescence transitions can be roughly estimated under the assumption that the gas is optically opaque to many of the resonance transitions. In contrast to IR pumping where the process occurs in a cascade of magnetic dipole transitions, UV pumping proceeds through many transitions ($\approx 10 - 20$) from the ground-state multiplet to upper-level multiplets. A detailed radiative transfer calculation is necessary given the transient nature of the GRB. Such a calculation is beyond the scope of this paper and will be the subject of a future work (Mathews & Prochaska, in prep). Here we present a simple framework for such calculations.

To estimate the number of far-UV photons absorbed per decay time, we first consider Si^+ . Adopting a column density $N(\text{Si}^+) = 10^{14.5} \text{ cm}^{-2}$ and Doppler parameter $b = 10 \text{ km s}^{-1}$ which roughly matches the profile of the excited gas for GRB 051111, we first produce a model spectrum of the ground-state Si II transitions with $912 \text{ \AA} < \lambda_{\text{rest}} < 2000 \text{ \AA}$ assuming the atomic data given in Morton (2003). We then measure the equivalent width of each si II transition which allows us to calculate the number of photons absorbed per second from the GRB afterglow spectrum (Equation 1). Summing over all of the transitions and evaluating the GRB afterglow at $t_{\text{obs}} = 50 \text{ s}$ and $r = 10 \text{ pc}$, we calculate the total number of photons absorbed per minute per ion

$$n_{\text{excite}}^{\text{UV}} = 80 \left(\frac{\langle L_{\nu=7\text{eV}} \rangle}{5.4 \times 10^{31}} \right) \left(\frac{r}{10 \text{ pc}} \right)^{-2} \left(\frac{N_{\text{ion}}}{10^{14.5} \text{ cm}^{-2}} \right)^{-1} \text{ min}^{-1} \quad (12)$$

assuming the unattenuated spectrum given by Equation 1. Although only a fraction of these photons will excite the Si^+ ions (roughly 66%), the rate is sufficiently high to show a modest Si II* column density at $r = 50 \text{ pc}$ at $t = 20 \text{ min}$ after the burst. Even at $r = 100 \text{ pc}$, there would be ≈ 16 excitations per ion prior to the onset of observations for GRB 051111. Therefore, we consider the excitation rate to be sufficient out to at least $r = 100 \text{ pc}$ from this afterglow.

We carry out similar calculations for O^0 and Fe^+ and find results that match Equation 12 to within a factor of 3 (Fe^+ has a higher rate and O^0 is lower, primarily reflecting the rest wavelengths of the resonance transitions). We emphasize that these excitation rates exceed IR pumping by more than an order of magnitude (compare Equations 11 and 12). Therefore, we conclude that indirect UV pumping is the principal excitation mechanism in GRB when photon pumping dominates.

We note that the excitation rate per ion given by Equation 12 is inversely proportional to the number of ions assumed. This is because the gas is optically thick in the majority of Si II transitions. The same holds for Fe II and O I transitions. Therefore, the equivalent width (hence, the number of photons absorbed) is insensitive to the column density assumed provided $N_{\text{ion}} \gtrsim 10^{14} \text{ cm}^{-2}$. Given the transient nature of the GRB, this has important implications for the excitation of these ions. Most importantly, for a gas cloud (or clouds) with total column den-

sity $N_{ion} > 10^{15} \text{ cm}^{-2}$, only a fraction of the gas along the sightline is excited prior to the onset of observations.

To zeroth order, the number of excited ions is given by the column density where the majority of transitions reach the saturated portion of the curve-of-growth. We have investigated this column density for the Fe^+ , Si^+ , and O^0 gas. We find that for $b = 10 \text{ km s}^{-1}$, the excitation saturates at $N_{ion}^{lim} \approx 10^{14.5} \text{ cm}^{-2}$ for Si^+ and Fe^+ and a few times larger value for O^0 . To first order, this limiting column density scales with the Doppler parameter of the gas, i.e. wider profiles should show larger column densities of excited gas when the excitation rate is limited by line saturation. We suspect that is not a coincidence that the column densities of excited gas in GRB 051111 and GRB 050730 are roughly consistent with this calculation.

In summary, UV pumping is a viable mechanism for excitations of the fine-structure states observed in GRB afterglow spectroscopy. For the case of GRB 051111, we find the gas would be pumped to at least 100 pc from the GRB afterglow if the far-UV light is not heavily attenuated by dust or intervening metal-rich gas. We draw similar conclusions for GRB 050730 and the other GRB listed in Table 3. In short, the radiation field of GRB afterglows is likely to excite Si^+ to at least 100 pc in the majority of systems observed to date.

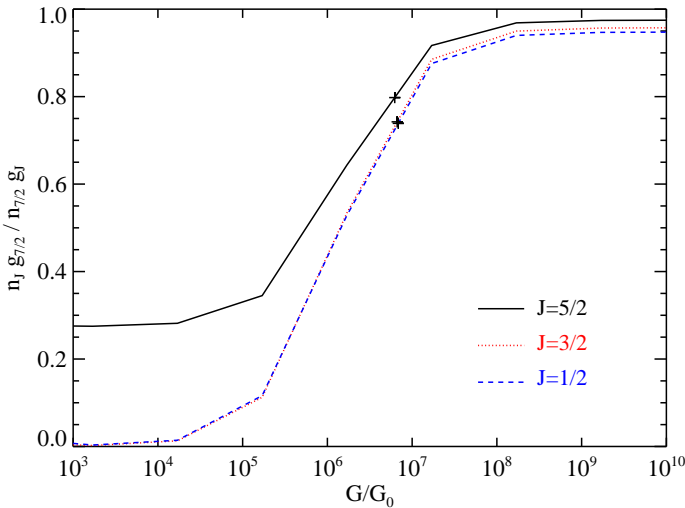


FIG. 8.— Indirect UV pumping of the Fe^+ excited levels relative to the $J = 7/2$ level (normalized by the degeneracy of the states g_J) as a function of the far-UV intensity. The levels saturate at high intensity, i.e., they are populated according to g_J . Also note that the $J = 3/2$ and $J = 1/2$ levels track one another at all intensity. This occurs because the two states require the absorption of two photons to be populated via UV pumping. The ‘+’ signs indicate the observed ratios of the excited levels for the gas toward GRB 051111. These observations are consistent with an intensity $G/G_0 \approx 10^{6.7}$.

While we have demonstrated that GRB afterglows are sufficiently bright to UV pump gas to large distance on short time-scales, we must also consider whether the relative populations of the excited states reproduce the observed ratios. In the next section, we will demonstrate that the Fe II excited levels for GRB 051111 are well described by a Boltzmann distribution with excitation temperature $T_{Ex} = 2600\text{K}$. Because UV pumping is not a thermal process, one does not expect a Boltzmann distribution aside

from the trivial case where the levels are saturated corresponding to $T_{Ex} \gg E_{J=1/2}/k$. Indeed, this is the case for GRB 050730. In Figure 8, we present the predicted abundances of the $J = 5/2, 3/2$ and $1/2$ levels relative to the $J = 7/2$ state normalized by the degeneracies g_J as a function of the far-UV intensity. In contrast with IR pumping, the spectral shape is unimportant to this calculation; the results only depend on the overall excitation.

An important prediction for UV pumping is that the $J = 3/2$ tracks the $J = 1/2$ level for all intensities. At $G/G_0 > 10^8$, the levels are saturated, i.e. populated according to g_J . At lower intensity $G/G_0 < 10^6$, the relative populations are strictly inconsistent with a Boltzmann distribution. For intermediate values ($G/G_0 \approx 10^{6.7}$), however, the differences from a Boltzmann distribution are small. The plus signs marked in Figure 8 show the observed ratios for GRB 051111 and indicate the data are well fit by a pumping scenario with a single intensity.

To conclude, we find that UV pumping can reproduce a Boltzmann distribution of Fe II levels with $T_{Ex} > 2000\text{K}$. A key prediction of UV pumping is that the relative population of the $J = 3/2$ and $1/2$ levels is given by the ratio of their degeneracies: $n_{3/2}/n_{1/2} = 2$. This is inconsistent with a Boltzmann distribution for $T_{Ex} < 1000 \text{ K}$ and is a direct test for distinguishing between collisional excitation and UV pumping: the observation of $n_{3/2}/n_{1/2} > 2$ would rule out UV pumping. In the cases of GRB 051111 and GRB 050730, however, we find that $n_{3/2}/n_{1/2} \approx 2$ and that both UV pumping and collisional excitation are viable mechanisms.

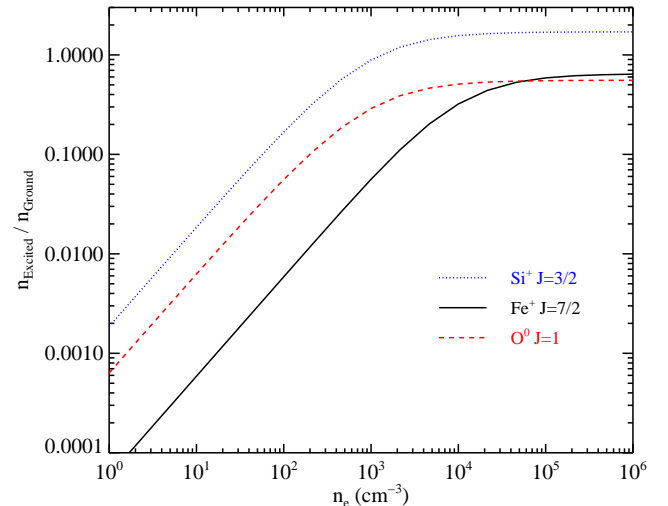


FIG. 9.— Collisional excitation of the first excited states relative to the ground state for Si^+ , Fe^+ , and O^0 versus the electron density. Note that for O^0 , neutral collisions dominate and we have assumed an ionization fraction $x = 10^{-2}$.

5.3. Collisional Excitation

The final excitation mechanism to consider is collisional excitation. For the Fe^+ and Si^+ ions, collisions with electrons are likely to dominate the rates⁹. For O^0 , the rates

⁹We caution that the neutral collision rates for Fe^+ have not yet been precisely calculated or measured in the laboratory.

for collisions with hydrogen atoms are much faster and are dominant for a mostly neutral cloud, i.e., $x < 10^{-2}$. The collision rates do vary with temperature but by less than an order of magnitude for temperatures $T = 100$ to 10000 K. In the following, we will present results for $T = 2600$ K.

In Figure 9 we present the population the first excited state relative to the ground state as a function of electron density n_e (neutral hydrogen density n_{HI} for O^0). The results are qualitatively similar to those for UV pumping (Figure 7) where one exchanges density with far-UV intensity. At large density, the excited states are populated according to their relative degeneracies although reduced by the Boltzmann function (see Equation 13 below). At low density, the population is proportional to the density of the colliding particle. Also, the excitation of Si^+ occurs at significantly lower density although note that the excitation of O^0 would be comparable for gas with low ionization fraction. In contrast to UV pumping, the excitation of Fe^+ requires significantly higher densities than Si^+ and O^0 . One finds $n_e > 10^5 \text{ cm}^{-3}$ for even a modest population of the $J = 7/2$ level.

When the collisional de-excitation rate $q_{ji}n_e$ exceeds the spontaneous decay rate A_{ji} , the excited states are populated according to a Boltzmann distribution,

$$\frac{n_i}{n_j} = \frac{g_i}{g_j} \exp[-(E_{ij}/k)/T_{\text{Ex}}] \quad , \quad (13)$$

where $E_{ij} \equiv E_i - E_j$ is the difference in energy between the two states, and T_{Ex} is the excitation temperature. Comparing predictions following Equation 13 with the observed column densities of ions at different excited states allows us to examine whether collisional equilibrium is a representative model for the excitation mechanism. A consistent fit in turn leads to a strong constraint for the gas temperature.

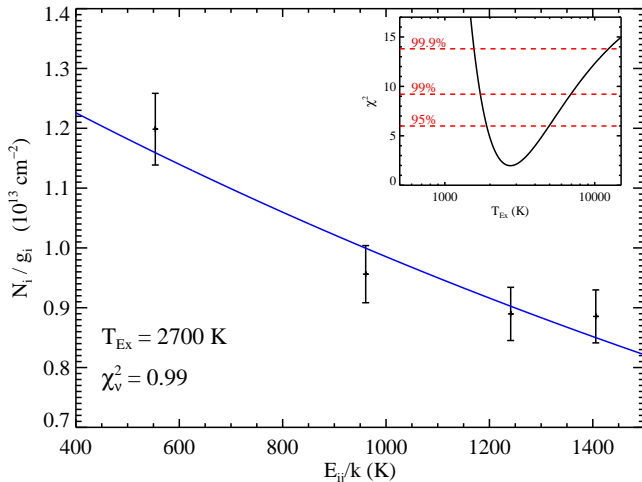


FIG. 10.— Plot of N_i/g_i for the Fe^+ excited states toward GRB 051111 as a function of their energy E_i above the ground state. Overplotted on the figure is the function $A \exp[-(E_{ij}/k)/T_{\text{Ex}}]$ for a minimum χ^2 value of $T_{\text{Ex}} = 2700$ K. The inset shows the reduced χ^2 values for the best fit for a range of T_{Ex} values.

Figure 10 shows for GRB051111 the observed column densities scaled by the corresponding degeneracy N_i/g_i for

the Fe II excited states as a function of the energy E_{ij} above the ground state $J = 9/2$. The error bars reflect $1-\sigma$ uncertainty in N_i . The modest decrease of N_i/g_i with E_{ij} suggests the levels are Boltzmann populated with an excitation energy greater than the largest E_{ij} value. The solid (blue) curve indicates the best-fit Boltzmann function with a best-fit excitation temperature $T_{\text{Ex}} = 2600$ K. The inset shows the minimum χ^2 values as a function of T_{Ex} ; the 99% c.l. limits are $T_{\text{Ex}}(99\%) = 1800 - 6000$ K. The reduced χ^2 is nearly unity, $\chi_v^2 = 0.99$, supporting the assumption that the Boltzmann function is a representative model.

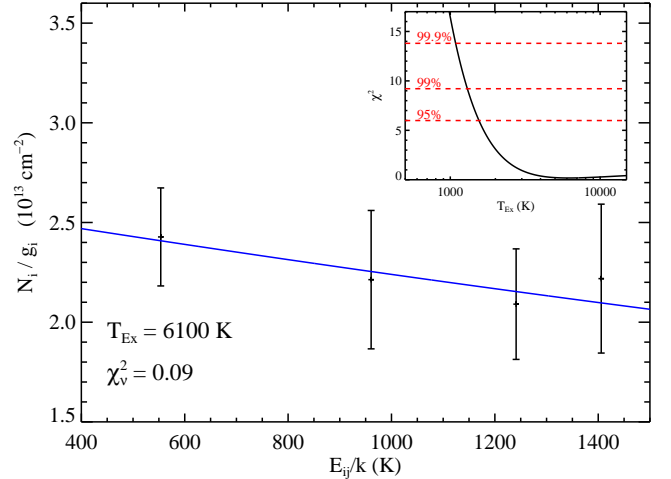


FIG. 11.— Same as Figure 10 except for GRB 050730.

We have repeated this analysis for GRB 050730 and the results are presented in Figure 11. The column density measurements have larger uncertainty and therefore place weaker constraints on T_{Ex} . Nevertheless, the Fe^+ excited state population is well fit by a Boltzmann function with $T_{\text{Ex}} \approx 6000$ K with a firm lower limit of 1000 K.

5.4. Summary

After examining the various mechanisms for exciting Fe II, Si II and O I excited levels in the presence of a GRB afterglow, we have demonstrated that indirect UV pumping and collisional excitation are both viable mechanisms for producing the excited ions. For indirect UV pumping to work, it requires an intensified far-UV radiation field: $G/G_0 > 10^6$. For collisional excitation to dominate, it requires a dense environment of $n_e > 10^3 \text{ cm}^{-3}$. We rule out IR pumping for gas at distances $\gtrsim 10$ pc and also find that the excitation rate is small compared to UV pumping at all distance (compare Equations 12 and 11). Therefore, the excitation of gas near GRB afterglows is primarily determined by indirect UV pumping and/or collisional excitation.

Another important conclusion is that the predictions for UV pumping and collisional excitation are very similar. For example, there is the trivial case at very high intensity or density where the excited levels are principally populated according to their degeneracy g_j , modified by the Boltzmann factor collisions. Although the detailed level

TABLE 4
TESTS OF UV PUMPING AND COLLISIONAL EXCITATION

Observation	UV Pumping	Collisions
$N_{J=3/2}(\text{Fe}^+) = 2N_{J=1/2}(\text{Fe}^+)$	Required	$n_e > 10^4 \text{ cm}^{-3}$, $T > 2500\text{K}$
Inverted Fe^+ population	Ruled out	$n_e < 10^3 \text{ cm}^{-3}$
Variability	Expected	Ruled out
Absence of atomic gas	Expected	Challenging
Overabundance of the Fe^+ $J = 9/2$ level	Expected	Challenging
$[N_{J=7/2}(\text{Fe}^+) - N_{J=3/2}(\text{Si}^+)] < [-1 + \epsilon(\text{Fe}/\text{Si})]^a$	Ruled out	Allowed
$N_{J=1}(\text{O}^0) < N_{J=3/2}(\text{Si}^+)$	Ruled out	Allowed for $x > 10^{-1}$
$N_{excited} > 10^{15} \text{ cm}^{-2}$	Pre-burst only	Allowed

^a $\epsilon(\text{Fe}/\text{Si})$ is the intrinsic, logarithmic Fe/Si gas-phase abundance allowing for nucleosynthetic and differential depletion effects.

populations are different because of the Boltzmann factor, one requires very high SNR observations to distinguish the cases if $T_{Ex} > 2000\text{K}$. In the next section, we will consider a few additional tests for distinguishing between the excitation mechanisms.

Regarding the gas near GRB afterglows, it is clear from Table 3 that photoionization dominates at distances less than 10 pc from the GRB and radiative processes are significant to 100 pc or further for the majority of afterglows. We conclude that circumstellar gas associated with the GRB progenitor will be excited by UV photons, if the gas is not entirely ionized by the event. Therefore, it is difficult to determine the density and temperature of such gas from the analysis of fine-structure transitions. A full calculation of the optical depth and time dependent processes of excitation are warranted and could help reveal the physical conditions in the absorbing medium (Mathews & Prochaska, in prep).

6. DISTINGUISHING BETWEEN PHOTON PUMPING AND COLLISIONAL EXCITATION

In the previous section, we argued that the excitation of fine-structure states of Fe^+ , Si^+ , and O^0 gas can occur along the sightline to GRB afterglows because of indirect UV photon pumping and/or collisional excitation. Each process has different implications for the physical conditions of the gas (e.g. density, temperature). It is therefore important to distinguish between the two mechanisms. We summarize a set of tests in Table 4.

There is a sufficiently large number of Fe II transitions covering a wide range of UV wavelengths in the rest frame and nearly every GRB afterglow spectrum includes the full set of Fe II excited levels (c.f. GRB 050730 and GRB 051111). Those sightlines which exhibit positive detections of the excited states allow different tests of the excitation mechanism; we consider the two cases separately.

6.1. When Excited States of Fe^+ are Detected

We have shown that under excitation equilibrium the indirect UV pumping scenario predicts a population ratio that is proportional to the degeneracy of the excited level, while the collisional excitation scenario predicts a population ratio that follows the Boltzmann function. In principle, one can therefore distinguish between these two excitation mechanisms based on the observed relative abundances between different excited ions. Our analysis has

shown, however, that measurement uncertainties often prohibit us from achieving the goal. Despite the caveat in obtaining more precise measurements, we highlight in this section two features that supports photon pumping and two features that supports collisional excitation for future studies.

Under photon pumping, we first note in Figure 8 that the $J = 5/2$ state is significantly more populated than the higher levels at low intensity $G/G_0 < 10^5$. This can be understood by the fact that one can populate the $J = 5/2$ and $J = 7/2$ states with a single photon whereas excitation to the $J = 3/2$ and $J = 1/2$ levels requires at least two-photon processes. Second, detection of line variability offers another discriminator between UV pumping and collisional excitation processes. For collisional excitation, we do not expect variability on time-scales that could conceivably be probed by GRB afterglows (i.e. less than a few days). In contrast, the absorption-line strength is expected to vary under photon pumping, because (1) Fe^+ becomes more ionized with time due to the afterglow; (2) the afterglow radiation field declines with time, leading to decreasing G/G_0 ; and (3) the diffusion of photons through an optically thick cloud is a time dependent process and could lead to both higher and lower column densities of the excited levels (Mathews & Prochaska 2006). To observe both features require that additional echelle observations be carried out at a later time.

We also note that in one extreme there is a maximum column density N_{max}^{UV} of ions that can be excited by UV pumping prior to the onset of spectroscopic observations, because of optical depth effects. The value of N_{max}^{UV} is primarily established by the velocity structure of the medium (i.e. the relative velocity of the absorbing clouds and their Doppler parameters) and to a lesser extent the size of the cloud ($1/r^2$ dimming). An accurate estimate of N_{max}^{UV} will require a time dependent radiative transfer calculation, but we note that nearly all of the Fe II, O I, and Si II transitions saturate at $N_{max}^{UV} \approx 10^{15} \text{ cm}^{-2}$. Therefore, if we observe a column density of excited gas significantly in excess of 10^{15} cm^{-2} , this would be strong evidence for collisional excitation, or possibly pre-burst UV pumping as optical-depth effects would not prevent the entire cloud from being excited (Sarazin, Rybicki & Flannery 1979).

Under collisional excitation, we first note that at the implied gas density $n_e > 10^3 \text{ cm}^{-3}$ (Figure 9) we also expect to observe large fractions of the elements C, Fe, and Mg

in their atomic states. Although we have shown in § 4.1 that the GRB afterglow can photoionize atomic gas at large distances, there is a relatively narrow window where the gas would be ionized and collisional excitation would dominate indirect UV pumping. Therefore, the presence of Fe^0 , Mg^0 , or C^0 may be viewed to support collisional excitation.

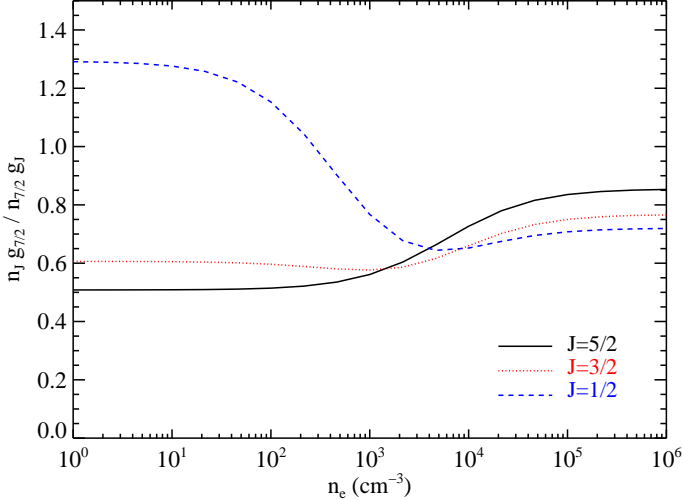


FIG. 12.— Collisional excitation of the Fe II excited levels relative to the $J = 7/2$ level normalized by the degeneracy of the states g_J as a function of the electron density. The levels saturate at high density, i.e., they become populated according to g_J weighted by the Boltzmann factor $\exp(-\Delta E/kT_{Ex})$ where we have assumed $T_{Ex} = 2600\text{K}$. Also note that at intermediate density the relative populations are roughly the same and that at low density the $J = 1/2$ and $J = 3/2$ exhibit an inverted population.

Second, we note in Figure 12 that under collisional excitation for a gas temperature $T_{Ex} = 2600\text{K}$ the population ratios between different excited levels are significantly different from the Boltzmann distribution at $n_e < 10^3\text{cm}^{-3}$. Specifically, both $J = 5/2$ and $3/2$ levels are significantly underabundant relative to the $J = 7/2$ level. In addition, the population becomes inverted, especially the $J = 1/2$ level. The relative abundance at these lower densities contrast with anything predicted for UV pumping. Although Figure 12 applies to a single phase of gas with $T = 2600\text{K}$, the results are similar for any temperature $T < 10000\text{K}$. It is, however, very challenging to observe an inverted population of Fe II levels because the absolute excitation rate of Fe^+ is small for $n_e < 10^3\text{cm}^{-3}$.

An intriguing aspect of the Fe II excited levels for GRB 051111 and GRB 050730 is the overabundance of the ions in the ground level. We also observed for GRB 051111 that the ground-state of Si^+ is at least $10\times$ more populated than the excited state. While one could construct a scenario which reproduces the observations for either excitation mechanism, we interpret the overabundance of the ground level as evidence for UV pumping for two reasons. First, the effect is naturally explained within the context of UV pumping by optical depth effects. If the cloud is optically thick, then one expects partial excitation especially if one cloud ‘shadows’ the rest of the gas that is further away from the afterglow. Second, the similarity in kinematics

suggest the gas is co-spatial and yet under collisional excitation the excited gas would require far greater pressure than is conceivable for the unexcited phase.

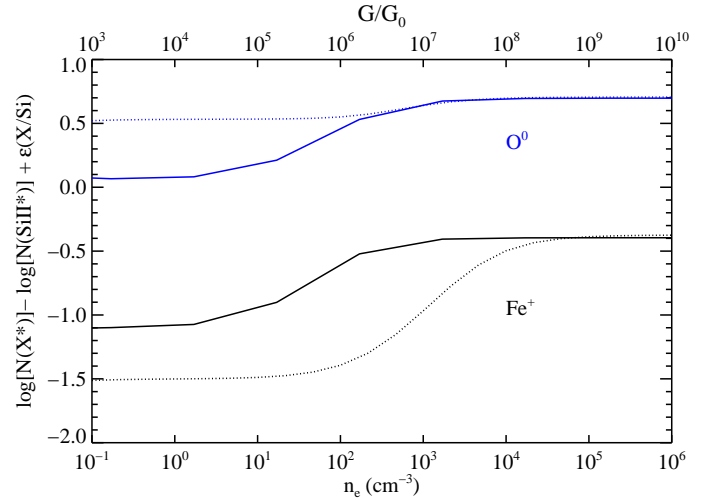


FIG. 13.— Comparison of the predicted column densities of the first excited states of Fe^+ (black) and O^0 (blue) relative to the $J = 3/2$ excited level of Si^+ for indirect UV pumping (solid curves) and collisional excitation (dotted; $T = 2600\text{K}$). We have assumed gas-phase abundances $\epsilon(\text{O}/\text{Si}) = 1$ and $\epsilon(\text{Fe}/\text{Si}) = 0$. It is important to note that the collisional excitation calculations for O^0 assume an ionization fraction $x = 10^{-2}$. Higher values of x would lead to lower $N(\text{OI}^*)$ values relative to $N(\text{SiII}^*)$ in a roughly linear fashion.

6.2. When Excited States of Fe^+ are not Detected

For GRB afterglows where the excited Fe II levels are not detected, the abundances of the first excited levels of O^0 and Si^+ , together with an upper limit in excited Fe^+ can be applied to constrain the excitation mechanism. Figure 13 presents the values of $N_{J=1}(\text{O}^0)$ and $N_{J=7/2}(\text{Fe}^+)$ relative to $N_{J=3/2}(\text{Si}^+)$ as a function of electron density and intensity for collisional excitation (dotted curves) and UV pumping (solid curves), respectively. Note that the curves assume that the gas-phase O^0 abundance is 10 times higher than Si^+ , $\epsilon(\text{O}/\text{Si}) \equiv \log N(\text{O}^0) - \log N(\text{Si}^+) = 1$, and that Si^+ and Fe^+ have equal gas-phase abundance, $\epsilon(\text{Fe}/\text{Si}) = 0$. Differential depletion, in particular, would modify these assumptions: increasing $\epsilon(\text{O}/\text{Si})$ and decreasing $\epsilon(\text{Fe}/\text{Si})$.

We first focus on Fe^+ and Si^+ . It is evident that collisional excitation at $n_e < 10^3$ allows for significantly lower values of $N_{J=7/2}(\text{Fe}^+)/N_{J=3/2}(\text{Si}^+)$ than UV pumping with $G/G_0 \leq 10^7$. The main result is that UV pumping does not allow $\log N_{J=7/2}(\text{Fe}^+) - \log N_{J=3/2}(\text{Si}^+) < [-1 + \epsilon(\text{Fe}/\text{Si})]$. Therefore, a GRB afterglow spectrum exhibiting Si II* absorption and strict upper limits on the excited Fe II transitions is likely to indicate collisional excitation. There are, however, two caveats. First, it assumes knowledge of the inherent Fe/Si ratio. In general, this may be inferred from the ground state populations. Second, the results in Figure 13 also assume steady-state conditions. The observations of GRB afterglows may occur on time-scales that are short compared to the lifetime τ_{life} of the excited levels (especially for Si^+ and O^0 which have $\tau_{\text{life}} = 1.3$ and

3.1 hr, respectively). Therefore, a significant underabundance of $N_{J=7/2}(\text{Fe}^+)$ relative to $N_{J=3/2}(\text{Si}^+)$ is possible from UV pumping if one observes the excited gas at a time when the excited Fe^+ ions ($\tau_{\text{life}} \approx 8\text{min}$) have decayed to the ground-state. In this case, of course, one would expect line-strength variability between early- and late-time spectroscopic data.

Next, we consider the O^0 and Si^+ predictions. Independent of the excitation mechanism, we find $N_{J=1}(\text{O}^0) \geq N_{J=3/2}(\text{Si}^+)$ for the assumed ionization fraction¹⁰, $x \approx n_e/n_H = 10^{-2}$. For a predominantly neutral gas, collisional excitation of Si^+ will roughly match that of O^0 and $N_{J=1}(\text{O}^0) > N_{J=3/2}(\text{Si}^+)$ is predicted. For larger values of x , however, the excitation rate for Si^+ is considerably higher and a significantly smaller ratio of $N_{J=1}(\text{O}^0)/N_{J=3/2}(\text{Si}^+)$ is expected. In fact, the only process which allows $N_{J=1}(\text{O}^0) < N_{J=3/2}(\text{Si}^+)$ is collisional excitation in a predominantly ionized medium, e.g. the Carina nebula in the Galaxy (Walborn *et al.* 2002).

7. DISCUSSION

7.1. Implications for GRB 051111 and GRB 050730

Despite different spectral coverage in the rest frame of GRB 051111 and GRB 050730, the echelle spectra of these afterglows exhibit ground-state Si^+ and Fe^+ features from all of their excited levels. In the case of GRB 050730, excited O^0 is also present. But due to measurement uncertainties, their population ratios may be explained by Boltzmann distribution with $T_{Ex} = 2600 - 6000\text{K}$ (Figures 10 & 11), as well as by UV pumping provided $G/G_0 \gtrsim 10^{6.5}$. We have investigated variations in the column densities and set *upper limits* to the line-strength variability of $< 10\%$ per 1800s for GRB 051111 and $< 30\%$ per 1800s for GRB 050730. It appears difficult to unambiguously rule out either UV pumping or collisional excitation as the dominant excitation mechanism. The only strong argument against collisional excitation is the absence of Fe^0 and C^0 atomic gas for GRB 051111 and GRB 050730, respectively.

Under collisional excitation, the excited ions occur irrespective of the presence of the afterglow and the gas is required to have $n_e > 10^5 \text{cm}^{-3}$ and $T \sim 2000 - 6000 \text{K}$ to populate the Fe II excited levels. If the excited gas arises from a layer of high density ($n_e > 10^5 \text{cm}^{-3}$), then based on the absence of Fe I we can place an upper limit on the ratio of the electron density to far-UV intensity $n_e \times (G/G_0)^{-1}$ (Equation 5). Adopting the best-fit Boltzmann distribution, we calculate the total Fe^+ column density $N_{\text{tot}}\text{Fe}^+ = 10^{14.4} \text{cm}^{-2}$, including all levels. Adopting a conservative upper limit to the atomic state $N(\text{Fe}^0) < 10^{12} \text{cm}^{-2}$ (Table 1) which accounts for continuum and statistical uncertainty, we therefore find from Equation 5 that $n_e \times (G/G_0)^{-1} < 1$ for $T < 10000\text{K}$. For $n_e > 10^5 \text{cm}^{-3}$, we find that $G/G_0 > 10^5$. Therefore, we conclude that we would only observe significant populations of the excited Fe II levels for gas in the presence of a strong far-UV radiation field.

To satisfy $G/G_0 > 10^5$, it requires the gas to lie within $\approx 0.1\text{pc}$ of a $T = 40000\text{K}$ O star with $R = 10R_\odot$. While

¹⁰This is a rough estimate of the ionization fraction for a predominantly neutral gas.

the GRB progenitor star is expected to reside in a star-forming region and therefore near other massive stars, we consider it highly unrealistic that the gas is at $> 100 \text{pc}$ from the GRB but also within 0.1pc of an O star.

A similar conclusion can be drawn for GRB 050730 using C I. We infer a C^+ column density by scaling $N(\text{Fe}^+) = 10^{14.8} \text{cm}^{-2}$ from the excited region with solar relative abundances: $N(\text{C}^+) = 10^{15.8} \text{cm}^{-2}$. The observed upper limit $N(\text{C}^0)/N(\text{C}^+) < 10^{-2.3}$ requires $G/G_0 > 5 \times 10^4$, again assuming a conservative limit to the temperature ($T < 10000\text{K}$). For GRB 050730, we have no significant constraint on the distance of the gas from the afterglow. But, if collisional excitation dominates indirect UV pumping (and that $n_e < 10^9 \text{cm}^{-3}$), then this gas must also be experiencing a strong local source of far-UV radiation. We conclude based on the null detections of atomic gas that *indirect UV pumping by GRB afterglow radiation is the dominant excitation process*.

We also note that there are additional challenges to a collisional excitation scenario. First, the gas would require a very large heating source to maintain the inferred temperatures for collisional excitation. For the implied physical conditions (e.g. $T = 2600 \text{K}$ and $n_e > 10^5 \text{cm}^{-3}$), [Fe II] cooling dominates. Using the coefficients given by Hollenbach & McKee (1989), we calculate a rate of $n\Lambda_{[\text{FeII}]} = 4 \times 10^{-23} \text{ergs s}^{-1} \text{H}^{-1}$ assuming 1/10 solar metallicity and that 90% of the iron is locked into dust grains. This implies a cooling rate $t_{\text{cool}} \sim kT/(n\Lambda_{[\text{FeII}]}) < 500\text{yr}^{-1}$. Including the cooling by meta-stable states of O I would imply an even shorter cooling time. Second, gas with $T \approx 3000 \text{K}$ is generally not stable to thermal perturbation. In the case considered here, the [Fe II] cooling curve is relatively insensitive to temperature variations but very sensitive to density changes. For example, an increase in n_H increases $n\Lambda_{[\text{FeII}]}$ and drives the gas to higher density and lower temperature until $T \ll 1000\text{K}$. Third, the implied pressure nT is extremely high. One would require a strong mechanical process (e.g. shock) to confine the gas and it would be surprising to therefore find the quiescent kinematic characteristics that are observed (Figures 1,2).

Adopting UV pumping as the the excitation mechanism, we can constrain the distance of the gas from the GRB based on known afterglow radiation field. For GRB 051111, the gas must arise at $r \approx 200 \text{pc}$. This distance is large enough to prevent the ionization of Mg^0 but also close enough that the Fe II and Si II levels would be UV pumped and also show the relative populations that are observed. In the case of GRB 050730, where the excited Fe II levels are populated according to their degeneracies g_J , the gas must lie within $\approx 100 \text{pc}$ of the afterglow (Table 3). The ionizing column of photons at 1pc is $6 \times 10^{22} \text{cm}^{-2}$. The gas is therefore not likely at $< 3 \text{pc}$, where the far-UV radiation field from the GRB afterglow will photoionize all of the C^+ , Si^+ , O^0 , and Fe^+ gas.

7.2. Implications of Fine-Structure Lines in Other GRB Afterglows

The detection of Si II* transitions is nearly ubiquitous in GRB afterglow spectra (Vreeswijk *et al.* 2004; Chen *et al.* 2005; Berger *et al.* 2005). This stands in stark contrast with intervening quasar absorption line systems where only C I* and C II* fine-structure lines have been

observed (e.g. Srianand, Petitjean & Ledoux 2000; Wolfe, Prochaska & Gawiser 2003; Howk, Wolfe & Prochaska 2005). To date, the observation of Si II* absorption for GRB have been interpreted as the result of collisional excitation and therefore evidence for large volume densities in the gas. We have demonstrated in this paper, however, that UV pumping is the most likely excitation mechanism if the gas is located within a distance of ≈ 100 pc. This conclusion holds for all of the GRBs with reported Si II* detections (Table 3) except for GRB 050408 (Foley *et al.* 2005). And, for sightlines exhibiting Fe II* absorption, we contend UV pumping is likely the only mechanism.

In summary, we conclude that in the presence of an intensified UV radiation field from the afterglow *indirect UV pumping alone offers a simple explanation for all the excited fine-structure transitions observed in GRB host environment to date without invoking extreme ISM properties*, such as high gas density. If we take the gas density allowed by the observed relative abundances of atomic species, $n_{\text{H}} = 100 - 1000 \text{ cm}^{-3}$ (§ 4.2), the observed large N_{HI} (e.g. Chen *et al.* 2005) implies a cloud thickness of 3–30 pc which is typical of giant molecular clouds (Turner 1988). In lieu of diagnostics from the fine-structure populations, one must rely on comparisons of the atomic states with higher ionization levels to constrain the gas density. We contend that the principal quantity inferred from the fine-structure lines is the distance to the GRB afterglow. At present, there is no obvious diagnostic for the gas temperature.

7.3. Implications for Gas Within 100 pc of GRB Afterglows

Our analysis reveals a number of implications for the study of gas located within 100 pc of the GRB afterglow. The first is that this gas may be identified by the absence of atomic absorption, in particular Mg I gas. Although the sightline is likely to penetrate Mg I gas at distances far from the GRB (e.g. within the galactic halo), differences in the line-of-sight velocities should distinguish these clouds. Therefore, a study of the kinematic differences between Mg I and Mg II profiles in GRB spectra is warranted.

In the absence of atomic gas (e.g. Mg I absorption) that coincides kinematically with the low-ion species, the gas may have small distance from the GRB afterglow and therefore may be circumstellar material from the progenitor. Unfortunately, the afterglow radiation washes out the most readily available diagnostics for studying the density and temperature of this gas. We note, however, that self-shielding of UV photons matching various excitation energies may be significant, especially for the majority of other GRB sightlines where the fine-structure column density is significantly lower than the ground-state (e.g. Vreeswijk *et al.* 2004; Savaglio & Fall 2004). We expect this may also be the case for GRB 051111 and GRB 050730. It is therefore possible that a significant portion of the gas is not excited by the afterglow and we could infer physical conditions for the bulk of the medium.

Another implication is that one must consider the fine-structure levels in the chemical abundance analysis. This will be especially important for sightlines with low total metal-line column density. The correction to $N(\text{Fe}^+)$ in GRB 050730, for example, is 33% and we estimate the

correction to $N(\text{Si}^+)$ is greater than 50%. If one cannot account for the excited-states in the analysis (e.g. because the lines are too saturated/blended for accurate measurement), then analysis of S^+ is preferred because it does not have fine-structure levels near the ground-state.

Finally, we emphasize again that to observe gas at 10 pc one requires a large pre-existing column density of neutral or partially ionized gas prior to the GRB event. This includes highly ionized species like C IV. Consider, as an example, the relatively spectacular C IV gas observed toward GRB 021004 which several authors have interpreted to arise from gas associated with the GRB progenitor (Schaefer *et al.* 2003; Mirabal *et al.* 2003; van Marle, Langer & Garcia-Segura 2005; Fiore *et al.* 2005). At $t_{\text{obs}} = 1$ hr after the GRB, we estimate an H I ionizing column density of 3×10^{21} photons cm^{-2} at 10 pc assuming the afterglow properties given in Table 3. This column significantly exceeds the N_{HI} value observed for the gas toward GRB 021004, therefore we assume that all of the low-ion gas within 10 pc was either ionized prior to the GRB or prior to the observations. This helps explain the absence of strong low-ion absorption¹¹. More importantly, the column density of C^{+3} ionizing photons with energy $h\nu = 64.5$ to 70eV at 10 pc is $\approx 10^{20} \text{ cm}^{-2}$. If this flux is unattenuated by gas within 10 pc then it would significantly ionize all of the C^{+3} ions within a few tens of pc from the GRB. At these energies, the principal source of opacity is He^+ , but we estimate that this gas will also have been burned away by the GRB and its progenitor. We contend, therefore, that the majority of C^{+3} gas observed along the GRB 021004 sightline is either associated with the larger star forming region and/or halo gas from the GRB host galaxy and/or its galactic neighbors.

The authors wish to recognize and acknowledge the very significant cultural role and reverence that the summit of Mauna Kea has always had within the indigenous Hawaiian community. We are most fortunate to have the opportunity to conduct observations from this mountain. We acknowledge the comments of an anonymous referee and also D. Hollenbach who stressed the importance of UV pumping. We are grateful to Grant Hill, Derek Fox and Barbara Schaefer for their roles in obtaining the Keck/HIRES data of GRB 050111 and I. Thompson for obtaining the Magellan/MIKE data of GRB 050730. The authors would like to thank C. McKee, N. Walborn, T. Gull, K. Sembach, A. Wolfe, B. Mathews, D. York, D. Welty, C. Howk, A. Konigl, and G. Blumenthal for helpful discussions. We thank Weidong Li, Nat Butler, and Dan Perley for providing preliminary results on the light curves of GRB 050111 and GRB 060206. We thank Miroslava Dessauges-Zavadsky for providing UVES measurements. J.X.P., H.-W.C., and J.S.B. are partially supported by NASA/Swift grant NNG05GF55G.

APPENDIX

PHOTOIONIZATION EQUILIBRIUM

Under steady-state conditions and photoionization equilibrium, the balance of photoionization and recombination for Mg^0 and Mg^+ gives

¹¹The observation of Al II absorption is an interesting exception.

$$n(\text{Mg}^0)n_\gamma c\sigma_{ph}^{\text{Mg}^0} = n(\text{Mg}^+)n_e [\alpha_r(T) + \alpha_{di}(T)] \quad (\text{A1})$$

where α_r and α_{di} are the radiative and dielectronic recombination coefficients and $\sigma_{ph}^{\text{Mg}^0}$ is the cross-section to photoionization integrated over the incident radiation field. For the recombination rates, we will use the fitting formula given by Aldrovandi & Pequignot (1973),

$$\alpha_r^{\text{Mg}^+}(T) = 1.4 \times 10^{-13}(T/10^4)^{-0.855} \text{cm}^3 \text{s}^{-1} \quad , \quad (\text{A2})$$

and Shull & van Steenberg (1982),

$$\alpha_{di}^{\text{Mg}^+}(T) = 4.49 \times 10^{-4} T^{-1.5} \exp(-5.01 \times 10^4/T) [1 + 0.0021 \exp(-2.61 \times 10^4/T)] \text{cm}^3 \text{s}^{-1} \quad . \quad (\text{A3})$$

For the photoionization rate, we integrate the Galactic far-UV radiation field determined by Gondhalekar, Phillips & Wilson (1980) over the fitting function for $\sigma_{ph}^{\text{Mg}^0}$ provided by Verner *et al.* (1996):

$$n_\gamma c\sigma_{ph}^{\text{Mg}^0} = \Gamma(\text{Mg}^0) = 6.8 \times 10^{-11} \frac{G}{G_0} \text{s}^{-1} \quad . \quad (\text{A4})$$

Although the radiation field for the gas associated with a GRB host galaxy will likely have a different spectral index than that of the Milky Way, the ionization rate is dominated by the photon density at $h\nu \approx 8 \text{eV}$ and, in any case, uncertainties in the atomic data limit the accuracy of this analysis to factors of a few. Rearranging Equations A1-A4 to express n_e in terms of the observed $N(\text{Mg}^0)/N(\text{Mg}^+)$ ratio we reproduce Equation 4.

One can derive a similar expression for Fe. In this case, radiation recombination dominates for $T < 8000\text{K}$,

$$\alpha_r^{\text{Fe}^+}(T) = 8.945 \times 10^{-9} \left[(\sqrt{T/0.04184}(\sqrt{T/0.04184} + 1))^{0.7844} (1 + \sqrt{T/5.35 \times 10^{13}})^{1.2156} \right]^{-1} \quad (\text{A5})$$

For the ionization rate we perform the same calculation as above (Equation A4) and find

$$\Gamma(\text{Fe}^+) = 1.7 \times 10^{-10}(G/G_0) \quad . \quad (\text{A6})$$

Finally, here are the relevant expressions for Carbon:

$$\alpha_r^{\text{C}^+}(T) = 7.651 \times 10^{-9} \left[(\sqrt{T/0.001193}(\sqrt{T/0.001193} + 1))^{0.1983} (1 + \sqrt{T/9.334 \times 10^{12}})^{1.8027} \right]^{-1} \quad (\text{A7})$$

and

$$\Gamma(\text{C}^+) = 6.6 \times 10^{-10}(G/G_0) \quad . \quad (\text{A8})$$

REFERENCES

- Aldrovandi, S. M. V. and Pequignot, D. 1973, *A&A*, 25, 137.
- Bahcall, J. N. and Wolf, R. A. 1968, *ApJ*, 152, 701.
- Barth, A. J. *et al.* 2003, *ApJ (Letters)*, 584, L47.
- Berger, E. *et al.* 2005, *ApJ*, in press (astro-ph/0511498)
- Bergeson, S. D. and Lawler, J. E. 1993, *ApJ*, 414, L137.
- Bergeson, S. D., Mullman, K. L., and Lawler, J. E. 1994, *ApJ*, 435, L157.
- Bergeson, S. D., Mullman, K. L., and Lawler, J. E. 1996, *ApJ*, 464, 1050.
- Bernstein, R. *et al.* 2003, in *Instrument Design and Performance for Optical/Infrared Ground-based Telescopes*. Edited by Iye, Masanori; Moorwood, Alan F. M. *Proceedings of the SPIE*, Volume 4841, pp. 1694-1704 (2003), 1694.
- Bloom, J. S. *et al.* 2002, *ApJ (Letters)*, 572, L45.
- Butler, N. *et al.* 2006, In prep.
- Cenko, S. B. and Fox, D. B. 2005, *GRB Coordinates Network*, 3834, 1.
- Charlton, J. C. and Churchill, C. W. 1998, *ApJ*, 499, 181.
- Chen, H.-W. *et al.* 2005, *ApJ*, 634, L25.
- Christensen, L., Hjorth, J., and Gorosabel, J. 2004, *A&A*, 425, 913.
- Churchill, C. W. *et al.* 2000, *ApJS*, 130, 91.
- Draine, B. T. and Hao, L. 2002, *ApJ*, 569, 780.
- Fiore, F. *et al.* 2005, *ApJ*, 624, 853.
- Foley, R. J. *et al.* 2006, *ApJ*, in press (astro-ph/0512081)
- Frisch, P. C. *et al.* 1990, *ApJ*, 357, 514.
- Frisch, P. C., York, D. G., and Fowler, J. R. 1987, *ApJ*, 320, 842.
- Gondhalekar, P. M., Phillips, A. P., and Wilson, R. 1980, *A&A*, 85, 272.
- Gull, T. R. *et al.* 2005, *ApJ*, 620, 442.
- Habing, H. J. 1968, *Bull. Astron. Inst. Netherlands*, 19, 421.
- Hall, P. B. *et al.* 2002, *ApJS*, 141, 267.
- Hill, G. *et al.* 2005, *GRB Circular Network*, 4255, 1.
- Hollenbach, D. and McKee, C. F. 1989, *ApJ*, 342, 306.
- Howk, J. C., Wolfe, A. M., and Prochaska, J. X. 2005, *ApJ*, 622, L81.
- Jenkins, E. B. 1996, *ApJ*, 471, 292.
- Lagrange-Henri, A. M., Vidal-Madjar, A., and Ferlet, R. 1988, *A&A*, 190, 275.
- Le Floch, E. *et al.* 2006, (astro-ph/0601252)
- Lipkin, Y. M. *et al.* 2004, *ApJ*, 606, 381.
- Mirabal, N. *et al.* 2003, *ApJ*, 595, 935.
- Mirabal, N. *et al.* 2002, *ApJ*, 578, 818.
- Morton, D. C. 1991, *ApJS*, 77, 119.
- Morton, D. C. 2003, *ApJS*, 149, 205.
- Nielsen, K. E., Gull, T. R., and Vieira Kober, G. 2005, *ApJS*, 157, 138.
- Paczyński 1998, in *Gamma Ray Bursts: 4th Huntsville Symposium*, volume 428, (Woodbury, New York: AIP), 783.
- Penprase, B. E. *et al.* 2005, *ApJ*, in press (astro-ph/0512340)
- Perley, N. *et al.* 2006, In prep.
- Perna, R. and Loeb, A. 1998, *ApJ*, 501, 467.
- Prochaska, J. 2005, *GRB Circular Network*, 4271, 1.
- Prochaska, J. X. and Wolfe, A. M. 2002, *ApJ*, 566, 68.
- Raassen, A. J. J. and Uylings, P. H. M. 1998, *A&A*, 340, 300.
- Ramirez-Ruiz, E. *et al.* 2005, *ApJ*, 631, 435.
- Rao, S. M. and Turnshek, D. A. 2000, *ApJS*, 130, 1.
- Sarazin, C. L., Rybicki, G. B., and Flannery, B. P. 1979, *ApJ*, 230, 456.
- Savage, B. D. and Sembach, K. R. 1991, *ApJ*, 379, 245.
- Savaglio, S. and Fall, S. M. 2004, *ApJ*, 614, 293.
- Savaglio, S., Fall, S. M., and Fiore, F. 2003, *ApJ*, 585, 638.
- Schaefer, B. E. *et al.* 2003, *ApJ*, 588, 387.
- Shull, J. M. and van Steenberg, M. 1982, *ApJS*, 48, 95.
- Silva, A. I. and Viegas, S. M. 2001, *Computer Physics Communications*, 136, 319.
- Silva, A. I. and Viegas, S. M. 2002, *MNRAS*, 329, 135.
- Srianand, R., Petitjean, P., and Ledoux, C. 2000, *Nature*, 408, 931.
- Stanek, K. Z. *et al.* 2003, *ApJ (Letters)*, 591, L17.
- Steidel, C. C. and Sargent, W. L. W. 1992, *ApJS*, 80, 1.
- Tripp, T. M., Lu, L., and Savage, B. D. 1996, *ApJS*, 102, 239.
- van Marle, A.-J., Langer, N., and Garcia-Segura, G. 2005, *A&A*, 444, 837.
- Verner, D. A. *et al.* 1996, *ApJ*, 465, 487.
- Vink, J. S. 2005, (astro-ph/0511048)
- Vogt, S. S. *et al.* 1994, in *Proc. SPIE Instrumentation in Astronomy VIII*, David L. Crawford; Eric R. Craine; Eds., Volume 2198, p. 362, 362.
- Vreeswijk, P. M. *et al.* 2004, *A&A*, 419, 927.
- Walborn, N. R. *et al.* 2002, *ApJS*, 140, 407.
- Welty, D. E., Hobbs, L. M., and Morton, D. C. 2003, *ApJS*, 147, 61.
- Wijers, R. A. M. J. 2001, in *Gamma-Ray Bursts in the Afterglow Era*, *Proceedings of the International workshop held in Rome, CNR headquarters, 17–20 October, 2000*, ed. Enrico Costa, Filippo Frontera, and Jens Hjorth, (Berlin Heidelberg: Springer), 306.
- Wolfe, A. M., Prochaska, J. X., and Gawiser, E. 2003, *ApJ*, 593, 215.
- Woosley, S. E. 1993, *ApJ*, 405, 273.
- York, D. G. and Kinahan, B. F. 1979, *ApJ*, 228, 127.